GFZ
Helmholtz Centre
POTSDAM

GeoMod2014

Modelling in Geosciences

Programme & Extended Abstracts

31 August - 5 September 2014

Editors:
Kirsten Elger
Øystein Thordén Haug
Malte Ritter

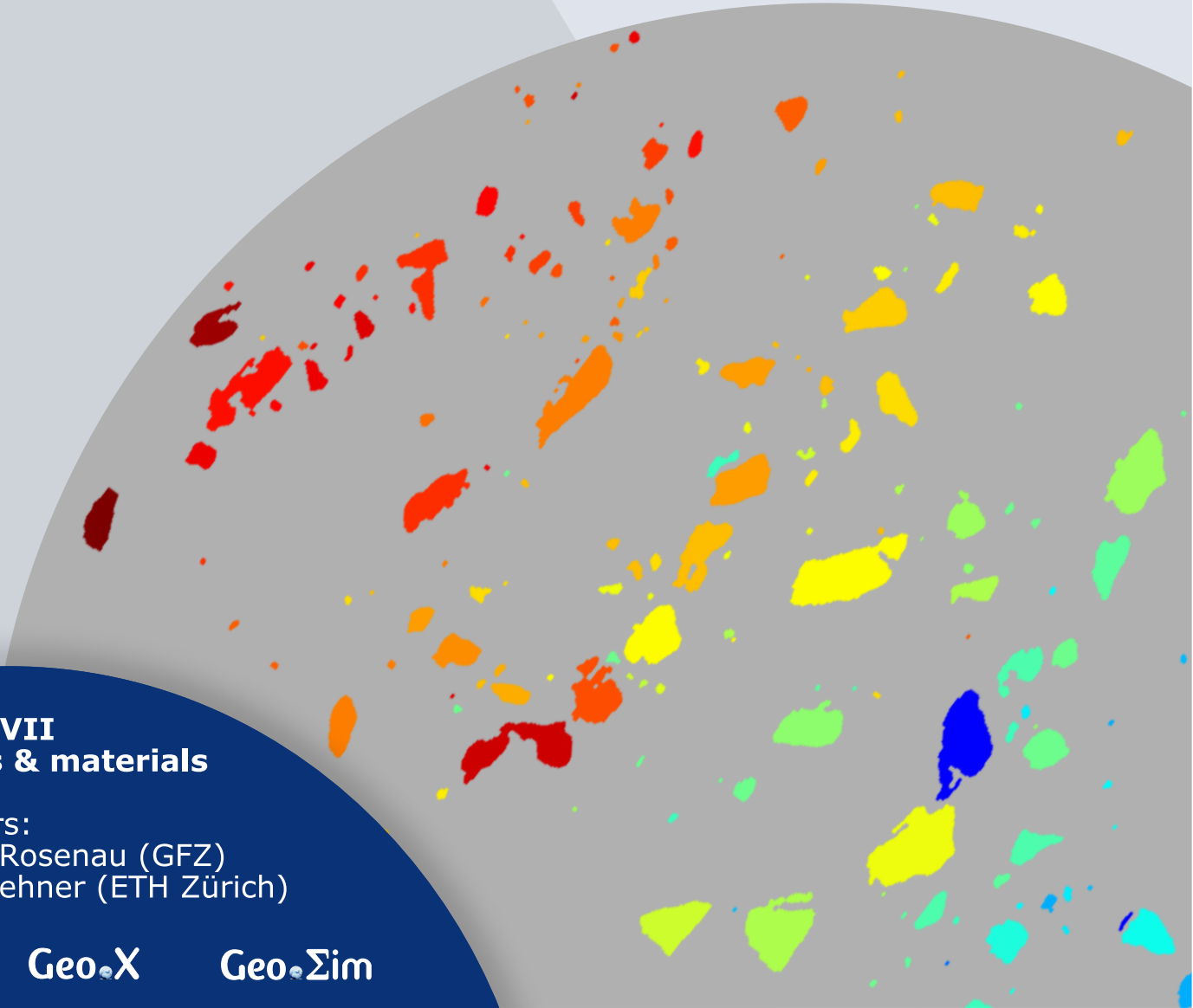

Session VII
Methods & materials

Conveners:
Matthias Rosenau (GFZ)
Marcel Frehner (ETH Zürich)

DFG GeoX GeoSim

Recommended Citation

Elger, K; Haug, Ø. T.; Ritter, M. C. (Eds), (2014): Proceedings of GeoMod2014 – Modelling in Geosciences: Programme and Extended Abstracts 31 August–5 September 2014, GeoMod2014 – Modelling in Geosciences (Potsdam 2014), Potsdam: GFZ German Research Centre for Geosciences. DOI: http://doi.org/10.2312/GFZ.geomod.2014.001.

Disclaimer and Copyright

Imprint

Publisher
Helmholtz Centre Potsdam
GFZ German Research Centre for Geosciences
Telegrafenberg
14473 Potsdam
Published in Potsdam, Germany

Editors
Kirsten Elger
Øystein T. Haug
Malte C. Ritter

doi: 10.2312/GFZ.geomod.2014.001

About this book

This volume contains the extended abstracts of contributions presented during GeoMod 2014 at the Helmholtz Centre Potsdam GFZ German Research Centre for Geosciences (GFZ Potsdam), showing the state of the art of the tectonic modeling community.

GeoMod is a biennial conference dedicated to latest results of analogue and numerical modelling of lithospheric and mantle deformation. It started in 2002 in Milan as RealMod2002, then moved to Lucerne (GeoMod2004), Florence (2008), Lisbon (2010), and Lausanne (2012).

GeoMod2014 took place from 31 August to 3 September 2014 with 138 participants from 25 countries on all continents. The scientific programme of GeoMod2014 was organized in seven topical sessions listed below. The conference was followed by a 2-day short course on "Constitutive Laws: from Observation to Implementation in Models" (including lectures, lab visits, and practical exercises), as well as a 1-day hands-on tutorial on the ASPECT numerical modelling software.

GeoMod2014 focused on rheology and deformation at a wide range of temporal and spatial scales: from earthquakes to long-term deformation, from microstructures to orogens and subduction systems. For the first time, the discipline of volcanotectonics was included, while the (mantle) geodynamics community was more strongly represented than in previous editions. The bridge to field geology has traditionally been strong. At GeoMod 2014, fitting to the focus on rheology, the rock mechanics community was also represented. We thank our sponsors DFG, GFZ Potsdam and Geo.X, the conveners and all participants for contributing to a successful conference.

The GeoMod2014 Committee

The Scientific Committee
Onno Oncken
Georg Dresen
Stephan Sobolev
Matthias Rosenau
Karen Leever

The Organising Committee
Kirsten Elger
Franziska Alberg
Students support: Zahra Amirzada, Felix Eckelmann, Øystein Thordén Haug, Shaoyang Li, Malte Ritter, Tasca Santimano, Sarah Schröder, Johannes Wagner

Sessions, Conveners, and keynote speakers

(Seismo-)tectonics
Conveners: Boris Kaus (U Mainz), Onno Oncken (GFZ/FU Berlin),
Keynotes: Kelin Wang (Geological Survey Canada, Alberta), Bertrand Maillot (U Cergy-Pontoise)

Tectonics & Surface Processes
Conveners: Fabien Graveleau (U Lille), Niels Hovius (GFZ/U Potsdam),
Keynotes: Ritske Huismans (U Bergen), Stéphane Dominguez (U Montpellier II)

Volcanism and Volcanotectonics
Conveners: Olivier Galland (U Oslo), Eoghan Holohan (GFZ)
Keynotes: Rikke Pedersen (U Iceland), Olivier Roche (U BP Clermont-Ferrand)

Geodynamics
Conveners: Francesca Funiciello (U Roma Tre), Stephan Sobolev (GFZ),
Keynotes: Anne Davaille (U Paris-Sud), Bernhard Steinberger (GFZ)

Rheology
Conveners: Georg Dresen (GFZ/U Potsdam), Hiroki Sone (GFZ),
Keynotes: Yuri Fialko (U California), Laurent Montési (U Maryland)

Fluids and Deformation
Conveners: Stephen Miller (U Bonn), Marcos Moreno Switt (GFZ),
Keynotes: Boris Galvan (U Bonn), Takeshi Tsuji (U Kyushu)

Methods and Materials (poster-only session)
Conveners: Matthias Rosenau (GFZ), Marcel Frehner (ETH Zürich)

Short course on "Constitutive Laws: from Observation to Implementation in Models"
Lecturers: Onno Oncken (GFZ Potsdam), Matthias Rosenau (GFZ Potsdam), Fabio Corbi (GFZ Potsdam), Georg Dresen (GFZ Potsdam), Stephan Sobolev (GFZ Potsdam), Sascha Brune (U Sydney)

Hands-on tutorial on "ASPECT: a next-generation geodynamic modelling software"
(Advanced Solver for Problems in Earth's ConvecTion)
Lecturers: Anne Glerum (Utrecht University), Juliane Dannberg (GFZ Potsdam). Supervised by Wolfgang Bangerth (Texas A&M University, ASPECT main developer), Stephan Sobolev (GFZ Potsdam), Bernhard Steinberger (GFZ Potsdam).

Contents

Session VII.

Methods and Materials

Session Description: Methods and Materials

Conveners: Matthias Rosenau (GFZ), Marcel Frehner (ETH Zürich)

In parallel to contributions to the thematic sessions of GeoMod 2014 we encourage all participants to present methodological advances in modelling, both analogue and numerical, in a special session which will consist of posters only. Contributions might include but are not limited to e.g. the development of new analogue materials, experimental setups, monitoring techniques as well as technical advances in mathematical approaches of simulation, analysis, visualization, data assimilation, etc.

Seismological monitoring of labscale landslides: Method & bouncing ball benchmark

Zahra Amirzada[1], Øystein Thordén Haug[1], Arnaud Burtin[1], Tuna Eken[1], Matthias Rosenau[1]

[1] *Helmholtz-Zentrum - GFZ Potsdam*
e-mail: *lg020@zedat.fu-berlin.de*
session: *Methods and Materials*

Introduction

Seismological monitoring of landslides, the remote detection and quantification of slope processes by seismometers, is an emerging field in earth and environmental science integrating geomorphological and geophysical methods (Petley, 2013; Burtin et al., 2013). The potential of the method is to invert seismic signals for a suite of aspects of event dynamics such as volume, velocity as well as details of the fragmentation process. For a sound interpretation of landslide signals in nature, knowledge of the responsible seismic sources and how the energy is transferred to the detector is paramount. However, because most events lack direct observations by other methods (e.g. cameras), the source-signal relationship remains often obscure. In order to shed light on the source-signal relationships in the context of seismological landslide monitoring, we started controlled laboratory experiments using analogue landslide models. Here we present the results of a first benchmark test including a controlled source, i.e. a ballistic steel ball impacting vertically a base made of various materials. This bouncing ball tests intend to calibrate and verify the monitoring method by relating a set of seismic metrics to the impact energy.

Benchmark setup & analysis

The benchmark setup allows a vertical free fall of a steel ball through air under earth's acceleration onto a horizontal base plate (glass, plastic, rubber) followed by several ball bounces. Steel balls of variable size (c. 1 – 10 mm diameter) are released from variable height above the base plate (<45 cm) in order to generate impact events covering a large range of energy (10^{-4} – 10^{-2}) Nm). The elastic deformation of the base plate in response to the impact is measured using triaxial capacitive accelerometers at a sampling frequency of 20 kHz. The potential energy of the steel ball is estimated from digital optical images of the impact taken at 250 Hz. We assume that the impact is perfectly elastic, i.e. that the difference in potential energy of the steel ball before and after the impact equals the impact energy which is transmitted and attenuated through the base plate and picked up by the sensors.

Signal processing includes: (1) low pass filtering the readings to <1500 Hz corresponding to the flat response regime of the sensors; (2) converting voltage to acceleration following a calibration procedure; (3) integrating the signal over time and high pass filtering to >100 Hz to retrieve the ground velocity (Figure 1).

Based on the ground velocity data start and end of the events were picked automatically using a standard STA/LTA trigger technique and the low pass-filtered Hilbert transform was used to derive the signal envelope. From the latter a series of seismic metrics following Dammeier et al (2011) were derived (Figure 1). These include:

- DUR: Duration of the event (s)
- RT: Risetime, i.e. time from start of event to velocity peak (s)

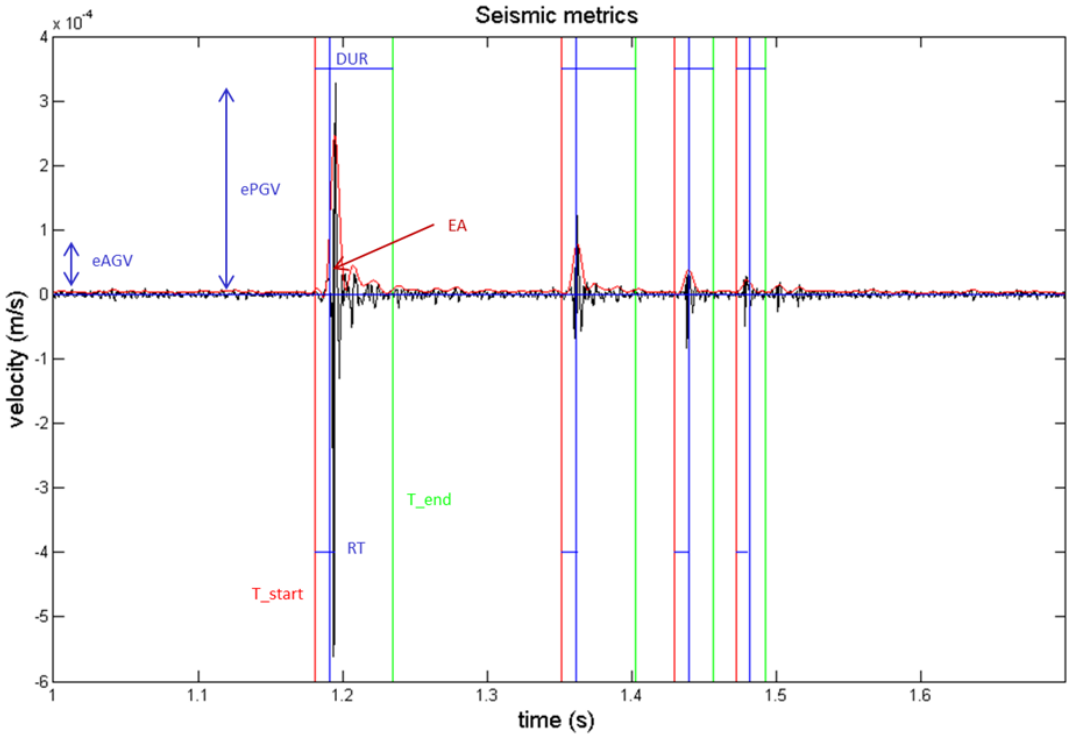

Fig. 1.: Example of "seismic" signal excited by successive impacts from a bouncing steel ball and recorded by an accelerometer in the benchmark setup. Seismic metrics according to Dammeier et al. (2011) indicated.

- ePGV: Peak ground velocity of signal envelope (m/s)
- eAGV: Average ground velocity of signal envelope (m/s)
- EA: Envelope area as a proxy for the energy of the triggering event (m)

Additionally, spectral analysis (Figure 2) based on the Fast Fourier Transform allowed quantifying the frequency content of the impact signal with high energy ("brightness") over time by means of the spectral centroid (SC in Hz).

Bivariate regression analysis finally has been used to find the relationships between the seismic metrics as defined above and the ballistic parameters, e.g. impact energy, in order to quantify the source-signal scaling relationships.

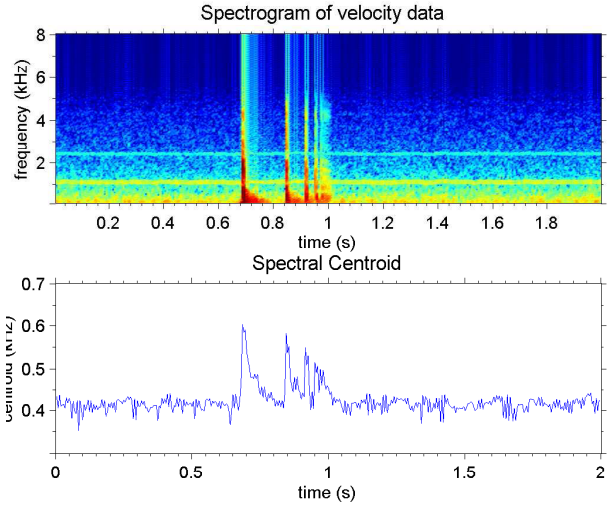

Fig. 2.: Spectrogram and spectral centroid of the bouncing ball signal in Figure 1. Note the decrease in centroid (= lowering the "tone") of successive impacts.

Scaling of seismic metrics to ballistic parameters & nature

Scaling, or similarity analysis, the comparison between the behavior of a labscale model and its natural prototype, helps to quantitatively relate labscale observation to nature and verifies the simulation method.

Our analogue models are generally setup at a length scale L*/L of 1:1.000 to 1:3.000 (i.e. a centimeter scales up to 10 – 30 meters). To assure dynamic similarity, the acting forces have to scale down consistently (Hubbert, 1937).

From this and Newton's 2nd Law ($F = m \cdot a$) it follows that for experiments conducted under earth's gravity field, all other accelerations in the model have to be same as in nature. Consequently, the time and velocity scales of the models both have to be the square root of the length scale, i.e.

$$T^*/T = v^*/v = (L^*/L)^{0.5} \sim 30 - 50 \quad (1)$$

We observe ground velocities and frequencies triggered by the ballistic impact in our setup that are in the order of $v^* = 10^{-4}$ m/s and $f^* = 10 - 1000$ Hz, respectively (Figure 1 and 2). According to (i) this scales to $v = 10^{-6}$ m/s and f = 1 – 20 Hz in nature which fits very well to observations (e.g. Burtin et al., 2013; Dammeier et al., 2011).

Preliminary analysis of a first set of experiments where we varied fall height of a 5 gram steel ball impacting glass, rubber and glass-on-plastic base plates shows positive correlations between the seismic metrics and fall height for all materials (Figure 3).

Data shown in Figure 3 indicate a linear correlation ($R^2 > 0.9$) between peak ground velocity, envelope area (as a proxy for energy) and fall height (as a proxy for impact energy). This verifies the potential of finding a simple relationship between impact energy and accelerometer response and marks the approach feasible.

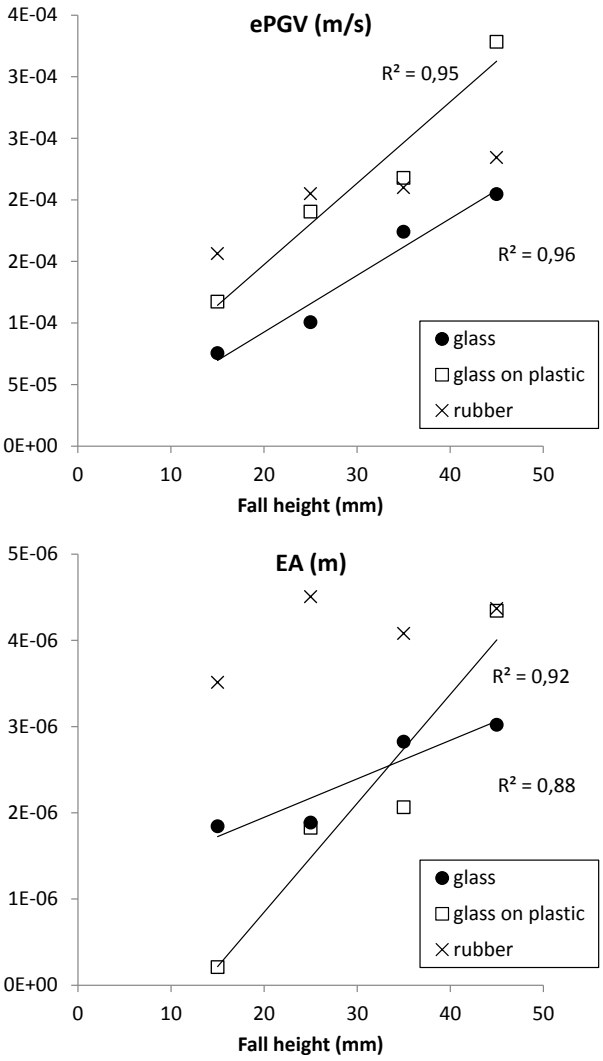

Fig. 3.: Relationship between seismic metrics (ePGV, envelope peak ground velocity, and EA, envelope area) and fall height of a 5 gram steel ball on various bases.

Outlook: Application to fragmenting labscale landslides & nature

Once we verified the monitoring method we plan to apply it to analogue models of fragmenting landslides. Preliminary test using loose sand avalanches versus cemented sand slides demonstrated the potential to differentiate between these two endmembers by means of their seismic signals and monitor the internal deformation and fragmentation process remotely. Besides having a new

monitoring technique for labscale experiments we aim at better understanding the signal-source relationship in nature. This includes questions revolving around the controls of the seismic energy released by gravitational mass movements: Which are the mechanisms contributing to the seismic signal (e.g. fragmentation, impact, sliding friction, collision)? What is their relative importance in the total and time variable seismic energy of an event? Can they be differentiated e.g. by the frequency domain they occupy?

References

Burtin, A., N. Hovius, D. T. Milodowski, Y.-G. Chen, Y.-M. Wu, C.-W. Lin, H. Chen, R. Emberson, and P.-L. Leu (2013), Continuous catchment-scale monitoring of geomorphic processes with a 2-D seismological array, Journal of Geophysical Research-Earth Surface, 118(3), 1956-1974, doi:10.1002/jgrf.20137.

Dammeier, F., J. R. Moore, F. Haslinger, and S. Loew (2011), Characterization of alpine rockslides using statistical analysis of seismic signals, Journal of Geophysical Research-Earth Surface, 116, doi:10.1029/2011jf002037.

Hubbert, M. K. (1937), Theory of scale models as applied to the study of geological structures, Geological Society America Bulletin, 48, 459-1520.

Petley, D. N. (2013), Characterizing Giant Landslides, Science, 339(6126), 1395-1396, doi:10.1126/science.1236165.

Small-scale modelling of ice flow perturbations induced by sudden ice shelf breakup

Giacomo Corti[1], Antonio Zeoli[2], Irene Iandelli[2]

[1] *Consiglio Nazionale delle Ricerche – Istituto di Geoscienze e Georisorse, Unità Operativa di Firenze, via G. La Pira, 4, 50121 Firenze, Italy*
[2] *Museo Nazionale Antartide, Università degli Studi di Siena, via del Laterino, 8, 53100 Siena, Italy*
e-mail: *giacomo.corti@igg.cnr.it*
session: *Methods and Materials*

Many glaciers in Greenland and Antarctica flow into the sea, terminating in extensive ice shelves which act as a buttress for their glaciers and slow their flow. A sudden marine shelf break up is expected to induce an increase in glacier speed, as flowing glaciers no longer encounter resistance on reaching the ocean, until a new equilibrium is established. The collapses of Antarctic Peninsula's Larsen-A and Larsen-B ice shelves between 1995 and 2002 confirmed these inferences. Glaciers draining the Larsen A ice sheet accelerated up to threefold after its 1995 collapse, whereas after disintegration of Larsen B ice shelf in 2002 some of the glaciers (Hektoria, Green and Evans glaciers) accelerated up to eightfold. Concomitant with the increase in velocity, glaciers significantly stretched and thinned close to their grounding line. These abrupt variations in the evolution of the glaciers have been mainly attributed to the removal of the buttressing ice shelf, a finding supported by the observation that glaciers that remained well buttressed by the remnant Larsen B shelf did not accelerate. This process can cause severe depletion of continental ice levels with obvious implications for eustatic sea level rise. Several numerical models have analyzed the process, but the complex boundary conditions adopted and the different modelling approaches make it difficult to isolate the role of ice-shelf buttressing on the large-scale dynamics of ice sheets, whose role thus remains controversial.

In this work we use simple small-scale laboratory models to reproduce the flow of a valley glacier draining an ice sheet into an ice shelf and to investigate the flow perturbations induced by ice shelf collapse. The analogue models, which apply to ice sheets grounded above sea level (e.g., East Antarctic Ice Sheet; Antarctic Peninsula and the Larsen Ice Shelf), were performed at the Tectonic Modelling Laboratory of CNR-IGG of Florence, Italy and at the Museo Nazionale Antartide, University of Siena, Italy. The flowing ice was simulated by using Polydimethilsyloxane (PDMS), a transparent Newtonian silicone that has been shown to well approximate the rheology of natural ice. Instability of glacier flow was induced by manually removing a basal silicone platform (floating on water) exerting backstresses to the flowing analogue glacier: the simple set-up adopted in the experiments isolates the effect of the removal of the buttressing effect that the floating platform exerts on the flowing glaciers, thus offering solid insights into the influence of this parameter on the flow perturbations resulting from a collapse event.

The experimental results show a significant increase in glacier velocity close to its outlet following ice shelf breakup, a transient effect that does not significantly propagate upstream towards the ice sheet, rapidly decays with time and is accompanied by significant ice thinning. This pattern closely matches the time-space evolution of flow perturbations observed on tributary glaciers of the Larsen B ice shelf after its 2002 collapse. Basal lubrication and variations in ice thickness do not significantly influence the process that

thus leaves the ice sheet almost unaffected by flow perturbations. Extrapolation of the experimental finding to the Larsen B case supports the importance of the removal of the buttressing effect on the dynamics of glaciers draining the Antarctic Peninsula. However, for reasonable values of ice thickness (typically <1000-1500m) the models indicate no propagation of the flow perturbation up to the ice sheet, suggesting that the removal of buttressing alone do not represent the major factor inducing depletion of ice sheets and threatening their stability, at least in case of valley glaciers for which the feeding ice sheet is grounded above the sea level (e.g., East Antarctic Ice Sheet; Antarctic Peninsula and the Larsen Ice Shelf).

Carbopol® for experimental tectonics: a rheological benchmark study

E. Di Giuseppe[1], F. Corbi[2], F. Funiciello[3], A. Massmeyer[4,5], T.N. Santimano[2]

[1]*Institut de Physique du globe de Paris, Sorbonne Paris Cite, Université Paris-Diderot, CNRS, 1 rue Jussieu, F-75005 Paris, France.*
[2]*Deutsches GeoForschungsZentrum GFZ, Helmholtz-Zentrum Potsdam, 14473 Potsdam, Germany.*
[3]*LET, Laboratory of Experimental Tectonics, Universita' 'Roma Tre', L.go S. Leonardo Murialdo, 1, 00146 Rome, Italy.*
[4]*RWTH Aachen, Lehrstuhl für Wärme- und Stoffübertragung, Augustinerbach 6, 52056, Aachen, Germany.*
[5]*Laboratoire FAST, CNRS/Université Paris Sud, Bat. 502 Rue du Belvedere, 91405 Orsay, France.*
e-mail: *digiuseppe@ipgp.fr*
session: *Methods and Materials*

Summary

As a prerequisite in experimental tectonics, in-depth analysis of the rheology of any analogue rock material is necessary to test its suitability for modelling a geophysical process in laboratory. Here we report a systematic characterization of physical and rheological properties of a large variety of polymeric hydrogels, known as Carbopol® , as a function of concentration, composition, pH, temperature and aging. These fluids feature a visco-elasto-plastic rheology which is described by the Herschel-Bulkley model. Benchmark tests are performed with three different types of rheometers at four institutes (FAST, GFZ, IPGP and LET), and a preliminary benchmark that tested the comparability of results is proposed.

Polymer rheology

Carbopol® identifies a polymer family based on modified crosslinked acrylic acid chemistry. Such polymers are available as fluffy white powders of 0.2-0.6 μm particles that absorb water, hydrate and swell creating a transparent gel-like texture if properly neutralized. The presence of neutralizer agents causes the creation of negative charges along the polymer backbone and, consequently, changes the interactions and the entanglements of its network. Therefore, when submitted to a stress τ, it deforms elastically when τ is lower than a critical value τ_y and is shear-thinning when $\tau > t_y$. Carbopol® polymers are commonly used in industry, i.e. cosmetic products, personal care and pharmaceutical merchandise, as thickeners, suspending agents and stabilizers. In the last years, Carbopol® has been employed in experimental tectonics and geodynamics including thermal convection experiments (e.g. Davaille et al., 2013), gravity-driven flow experiments (e.g. Chambon et al., 2013), and strain localization experiments (Schrank et al., 2008) because of its versatility to provide a large range of yield stress values and shear thinning behavior, and excellent transparency. Satisfying the rheological similarity criteria is a great advantage for modelers, but at the same time characterizing Carbopol® rheology is complex, requires time-consuming efforts, and the results may be affected by several physical parameters. This limited the use of this material in the last years.

Conscious that a deep knowledge of the physical and rheological properties of the working

fluid is pivotal for modeling properly a geophysical process, we decided to carry out an extensive study of the rheology of different Carbopol® types as a function of concentration, composition, pH, temperature and aging. Their flow behavior is described as well as their visco-elastic VE properties.

Selected Carbopol® samples, methods and rheometers

Here we report rheological measurements of six different types of Carbopol® , namely: ETD2050, ETD2623, Ultrez10 (U10), Ultrez21 (U21), EZ2, EZ3. Our selection aims at covering the widest range of rheological behaviour according to preliminary data provided by the producing company (*Lubrizol* – http://www.lubrizol.com) and the ease of preparation. The samples have been prepared at intermediate to high concentrations, ranging from 0.1 to 1.0 wt%. All the samples have been prepared following a standard procedure including neutralization (pH = 7) to always work with the maximum viscosity. The viscous behaviour and yield stress are evaluated by means of rotational and oscillatory tests.

In a first set of tests, we imposed a torsional flow to the sample in a rotational regime. The rheological tests consist of imposing a wide range of shear rate ($\gamma = 106{-}3 - 10^3$ s^{-}1) and measuring the stress (i.e. strain rate controlled) or vice-versa (i.e. stress controlled). Each flow curve is then fitted with a Herschel-Bulkley (HB) model, a rheological model that successfully describes Carbopol® flow properties. This procedure allows the estimation of the amount of stress that the sample experiences before yielding, τ_y, the flow index n (that describes degree of shear thinning), and sample consistency, K_y (a constant of proportionality between stress and strain rate).

A second set of tests in oscillatory regime are used to examine the VE behavior of Carbopol® . The standard procedure adopted in Material Science consists of measuring the energy stored in the sample during deformation and the energy lost afterwards. These two quantities are expressed, respectively, by the storage (G') and the loss (G") moduli, over a broad range of deformation and deformation rates (Mezger, 2002). The amplitude sweep test applies shear strain amplitude, γ, ranging between 10^{-2} and 10^3 % at constant frequency ($\omega = 1$ s^{-1}). The plateau of the G' curve determines the linearity of the VE behavior and its threshold γ_{LVE}, that is the amount of strain after which the sample structure is irreversibly changed. The *frequency sweep test* applies a constant amplitude oscillation (where $\gamma < \gamma_{LVE}$) with frequency ranging from 10^2 to 10^{-2} s^{-1}. The region in the frequency domain where the G' intersect the G" curve is equivalent to the Maxwell relaxation time, while the elastic shear modulus is identified as the value of G' obtained at the highest frequencies, where the plateau is reached.

This benchmark study has been conducted in synergy between four laboratories equipped with different rheometers. Rheometric measurements at the IPGP are performed on a RheoStress RS60 (ThermoHAAKE). Measurements at FAST are performed on a Physica MCR501 (Anton Paar). Measurements performed at LET and GFZ are performed on a Physica MCR301 (Anton Paar). All the rheometers employed in this study, are equipped with a Peltier element to control the temperature and with a solvent trap to minimize sample evaporation. The measurement systems used vary between the different labs and include plate-plate and cone-plate geometries as well as different surface roughness (sandblasted, polished).

Carbopol® ETD2050 benchmark

Samples of 1.0 wt% Carbopol®ETD2050 are prepared following a standard procedure in each laboratory. All the Peltier elements are set at T = 23 °C, which is the typical room temperature in laboratory. Viscosity and shear stress values obtained by the different rheometers are in very good agreement for $\dot{\gamma} > 1$ s^{-1} (Fig.1). However, assessment of τ_y provides larger variability, i.e. τ_y undergoes a variation up to a factor

of 3. We attribute this variation to the different measurement system geometries (i.e. plate-plate vs. cone-plate) adopted that may cause wall slip and/or transitional effects. Measurements carried out with the oscillatory methods to assess the viscoelastic behaviour of our samples show a much better reproducibility. Both amplitude and frequency sweep tests reveal an excellent agreement of measurements of the G' and G" moduli on the different rheometers. G' measured in amplitude sweep test with MCR301 (LET) shows the same values measured with the MCR501 (FAST), but differs by 7 % from the curve obtained with the same device (MRC301 - GFZ), and by only 3 % from data obtained with RS600 (IPGP). G" variability is in the same range and $\gamma_{LVE} =$ 10 % for all measurements. For the frequency sweep test, G' measured with MCR301 (LET and GFZ) shows a difference of almost 20 %, while there is a difference of 5 % between RS600 (IPGP) measurements and MCR301 (GFZ). Despite some uncertainty of τ_y in rotational tests, we consider our benchmark successful and conclude that Carbopol® allows in general to obtain reproducible results if preparation follows a strict procedure.

Systematics of Carbopol® rheology: Effects of concentration, composition, pH, temperature and aging.

Effect of concentration:

The viscosity curve of ETD2050 and ETD2623 exhibit an increase of approximately two orders of magnitude as the concentration is increased from 0.1 to 1.0 wt% accompanied by an increase of the shear thinning behaviour. U10 viscosity increases by 2 orders of magnitude as concentration increases from 0.1 to 0.5 wt%, and 3 orders of magnitude as concentration increases from 0.5 to 1.0 wt%. ETD2050 linear viscoelastic range increases by 6 times when concentration increases from 0.1 wt% to 1.0 wt%. An increase of concentration of the same amount provokes an increase of the linear viscoelastic range of about 16 times for U10 and ETD2623. Independently of the type of Carbopol® , increasing the concentration causes an increase of the viscosity and shear thinning behaviour, of γ_{LVE} and G'.

Effect of composition:

The composition of the molecules forming the Carbopol® gels strongly affects their rheology. At low concentration, 0.1 wt%, both ETD samples show higher viscosity and G' modulus than Ultrez samples. An inverse behavior is observed at higher concentration, i.e. 1.0 wt%: Ultrez and EZ samples show a similar flow behavior, ETD2050 reaches the lowest viscosity values and ETD2623 curves have intermediate values. Storage modulus attains the highest values for Ultrez and EZ samples.

Effect of pH:

Non-neutralized samples have a pH ranging between 2.5 and 3.5 and have very low viscosities, especially ETD and Ultrez. Independently from Carbopol® composition, the viscosity has the highest values for pH in the 6 to 9 range. The viscosity decreases for pH values above 9.0. Actually, adding a large amount of neutralizer causes an excess of electrolytes that produces the moistening of the electrostatic repulsions.

Effect of temperature:

Our results show an inverse relationship between temperature and viscosity. For T varying between 15 and 40 °C, the viscosity decreases by 30% for ETD2623 (0.1 and 1.0wt%) and U10 (0.1 wt%), U21 (0.1 wt%) viscosity is more sensible to temperature with a reduction of 46% in the same temperature range, while ETD2050 viscosity (0.1 wt%) is less sensible with a viscosity reduction of 10%.

Effect of aging:

According to technical sheets, Carbopol® polymers are very stable in time, however we suggest

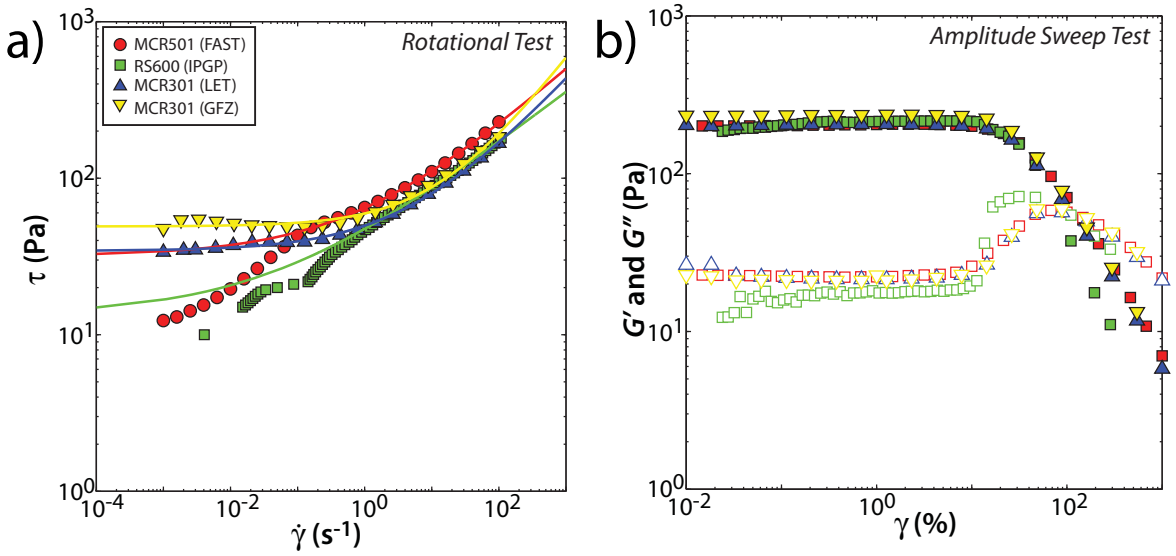

Fig. 1.: Results of the benchmark tests performed on ETD2050 Carbopol® samples of 1.0 wt% and T = 23 °C. a) Results of the flow test (rotational regime): shear stress versus shear rate; b) results of amplitude sweep test (oscillatory regime): G' and G" moduli versus deformation amplitude. Symbols identify the laboratory and the rheometer used for the benchmark. Filled symbols mark the storage modulus G', open symbols the loss modulus G".

using this material within a few days after preparation. Our measurements 2.5 - 5 weeks after samples' preparation revealed a decrease of viscosity values by almost 30% for samples with concentration 0.1 wt% anddecrease of 10% for samples with concentration 1.0 wt%.

References

Chambon, G., Ghemmour, A., Mohamed, N., 2013. Particle migration within free-surface flow of a viscoplastic flow. EGU General Assembly.

Davaille, A., Gueslin, B., Massmeyer, A., Di Giuseppe, E., 2013. Thermal instabilities in a yield stress fluid: existence and morphology. J. Non-Newtonian Fluid Mech. 193, 144-153.

Mezger, T., 2002. The Rheology Handbook: For Users of Rotational and Oscillatory Rheometers. Vincentz Verlag Hannover.

Schrank, C., Boutelier, D., Cruden, A., 2008. The analogue shear zone: From rheology to assoiciated geometry. J. Struct. Geol. 30, 177-193

Initiation process of the frontal thrust revealed from detailed analogue experiments

T. Dotare[1], Y. Yamada[1,2], T. Hori[2], H. Sakaguchi[2]

[1] *Graduate School of Engineering, Kyoto University, Kyoto, Japan*
[2] *Japan Agency for Marin-Earth Science and Technology (JAMSTEC), Yokohama, Japan*
e-mail: *dotare.tatsuya.76s@st.kyoto-u.ac.jp*
session: *Methods and Materials*

Summary

Discontinuity surfaces (e.g. fractures, faults) in rocks significantly influence fluid permeability, thus their distributions have to be evaluated in detail for hydrocarbon exploration / production. To establish a fracture distribution model, a series of analogue experiments were conducted and the fault initiation process in the experiments was analyzed in detail by using a digital image correlation technique. The result of our shortening experiments identified a number of weak shear bands prior to the later initiation of a frontal thrust. Such minor shear bands have been reported in the toe area of the Nankai accretionary prism, SW Japan. By comparing with several transects at this subducting margin, we can classify lateral variations in the structural geometry into deformation stages we identified in the models.

Introduction

Discontinuity surfaces, such as fractures and faults, have been an important target of oil and gas exploration and production. Recent hydrocarbon production from shale requires detecting areas of better initial permeability, can be regarded as 'sweet spots', due to rich discontinuity surfaces. Such surfaces are generally of subseismic scale and hard to detect from surface investigations.

Analogue modeling is a useful tool for evaluating how geologic structure is formed and constructing detailed structural models including minor deformation features. In recent study, digital image correlation technique (e.g. DIC) enables us to detect the deformation in the analogue model quantitatively and in high spatial and temporal resolution. Previous studies demonstrated that this technique can reveal detailed styles of strain accumulation in analogue models (e.g., Adam et al., 2005, Hoth et al., 2007), and the technique is now widely applied to analogue experiments to reveal structural evolution quantitatively.

In this study, we aimed to observe small scale structures (i.e. fractures or minor faults) developed during deformation process in shortening experiments. Our observations focused on the frontal thrust area whose detailed deformation was analyzed with DIC technique.

Experimental setup

The setup of our shortening experiments is summarized in Figure 1. The experimental material is beach dry sand (Toyoura sand) and its cohesion is ca 100Pa. Scaling factor is $10^4 \sim 10^5$. During shortening the material, deformation at the frontal thrust was recorded every 27μm shortening. (Figure 2), with two digital cameras (cannon EOS 7D) through a transparent side-wall.

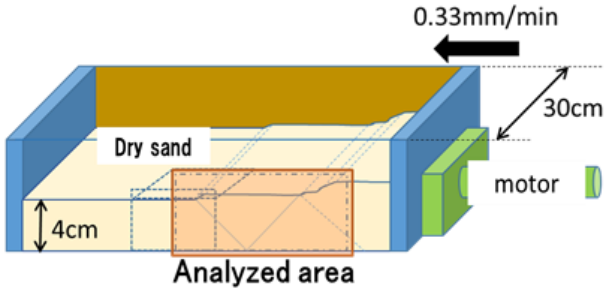

Fig. 1.: Experimental setup

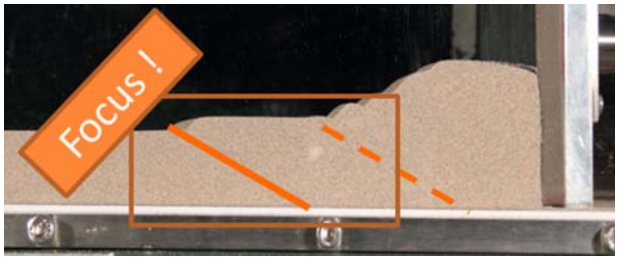

Fig. 2.: Analyzed area

Experimental results

When the old (pre-existing) frontal thrust is active (a in Figure 3 and 4), shear strain shows a constant value. After this, the activity of the old (pre-existing) frontal thrust decreases (b in Figure 4), and several weak shear-strain bands appeared in front of the old thrust (Figure 3b). The activity of each band is very short (can be detected in only 1 or 2 snapshots), and locations are systematically but rapidly changing. Then, the shear bands starts to localize at a specific location (Figure 3c) and the shear strain along the old thrust significantly decreases (c in Figure 4). Finally, the activity of the weak shear bands ceases and a new frontal thrust is generated showing a constant value of shear strain (d in Figure 3 and Figure 4)

Discussion and implication to real geology

From our experimental results, we can divide the initiation process of the frontal thrust generation into three stages:

Stage 1: Deformation propagating stage (b in Figure 3 and Figure 4). Characterized by short-life minor "weak shear bands" in front of the old frontal thrust of decreasing activity.

Stage 2: Strain localizing and thrust initiation stage (c in Figure 3 and Figure 4). The shear strain starts to localize and the location of the new frontal thrust seems to be selected among previous minor weak shear bands during the localizing process.

Stage 3: Active frontal thrust stage (d in Figure 3 and Figure 4). The newly initiated thrust is the only active fault showing a constant strain value. No weak shear band observed.

As a natural example, we have looked at the proto thrust zone (PTZ) at the toe of the Nankai accretionary prism, SW Japan. The Nankai accretionary prism is formed by the subduction of the Philippine Sea plate underneath the southwest Japan arc (Eurasian plate) and active sediment accretion is presently taking place (Moore et al., 2001). It has been reported that the structural domain varies between two parallel transects; Ashizuri and Muroto transects. While the Ashizuri transect has a well-developed PTZ containing a series of subparalell dipping discontinuities (Figure 5 Toe of Ashizuri Transect (Morgan et al., 1995)Figure 5), the Muroto transects has a few discontinuity features and narrow proto-thrust zone (Moore et al., 2001) (Figure 6). Moore et al. (2005) also attributed these variations to differences in mechanical properties and/or pore pressures, but this has not been confirmed.

Based on the deformation stages as proposed above, the sub-parallel discontinuities may correspond to the 'weak shear bands' observed in experimental results, and the along-strike variation may be not due to the mechanical property but the initiation stages of the frontal thrust. Since the surface topography of the Muroto transect PTZ is more deformed than that of the Ashizuri transect, the Muroto PTZ is in the later stage; i.e. the Ashizuri PTZ may be in the Stage 1, Muroto PTZ may be in the Stage 2. The Muroto PTZ could have been wider in the past with more discontinuity surfaces but now these minor features may have all disappeared and cannot be

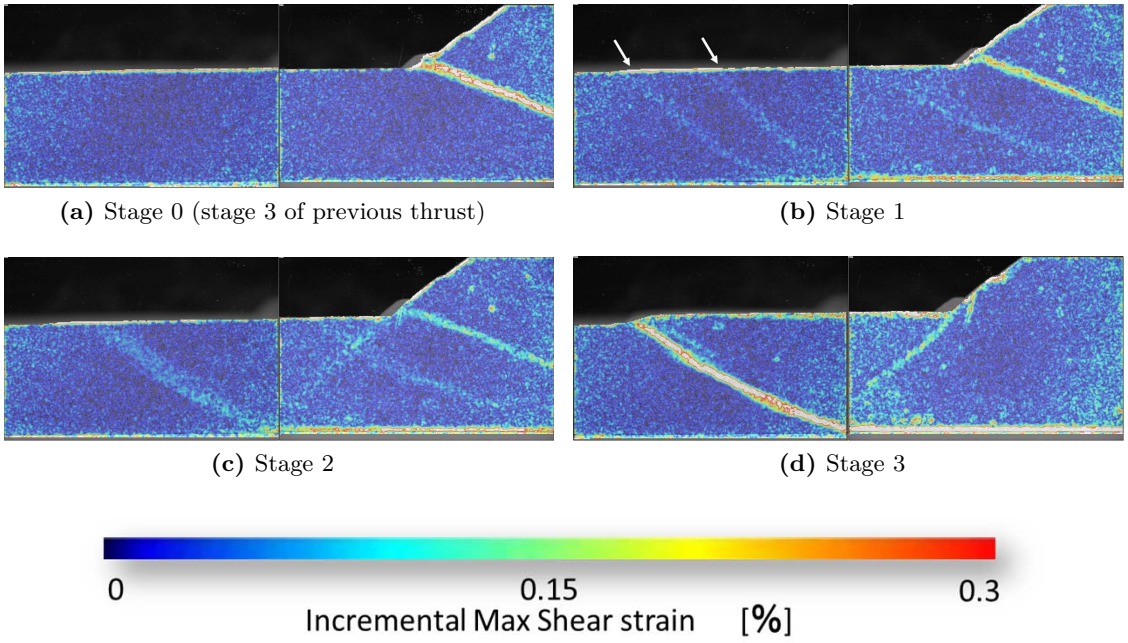

(a) Stage 0 (stage 3 of previous thrust)

(b) Stage 1

(c) Stage 2

(d) Stage 3

(e) Stage 2

Fig. 3.: Snapshots of experimental results. (a) ∼ (d) correspond to deformation stages. Each picture shows the incremental max shear strain distribution calculated every 27μm shortening.

detected.

Moore et al (1995) mentioned that the Cascadea accretionary margins PTZ has a lot of subparallel protothrusts with some negative-polarity reflection in the seismic dataset. This suggests possible fluid migration along these faults. During Stage1, 'weak shear bands' rapidly change their location and may develops a lot of subparalell active protothrusts, but previous protothrusts became inactive once the frontal thrust initiated. Fluid migration paths may focus on the new active frontal thrust and previous protothrusts may not show clear seismic anomaly (negative-polarity). This assumption is consistent with the different deformation stage of Ashizuri (Stage1) and Muroto (Stage2) protothrust zones.

Conclusion

We conducted the detailed analogue sandbox modelling focusing on the initiation of the frontal thrust, and found 'weak shear bands' before new fault initiates and strain concentration at the area of the new thrust formation. By comparing to the toe geometry at the Nankai accretionary prism, we inferred the along-strike variation of structural geometry may be due to the different deformation stages.

References

Adam, J. et al.; 2005: Shear localization and strain distribution during tectonic faulting—new insights from granular-flow experiments and high-resolution optical image correlation techniques. Journal of Structural Geology, 27(2), 283–301.

Hoth, S. et al.; 2007: Frontal accretion: An internal clock for bivergent wedge deformation and surface uplift. Journal of Geophysical Research, 112(B6), B06408.

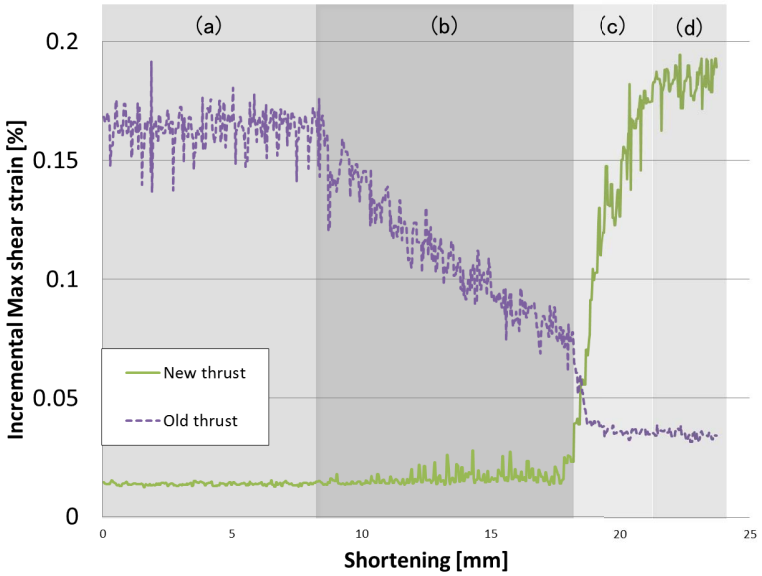

Fig. 4.: Time series of old and new thrust activation (incremental shear strain). (a) (d) correspond to Figure 3. Each value are calculated around 1cm×1cm square area where both thrusts intersect.

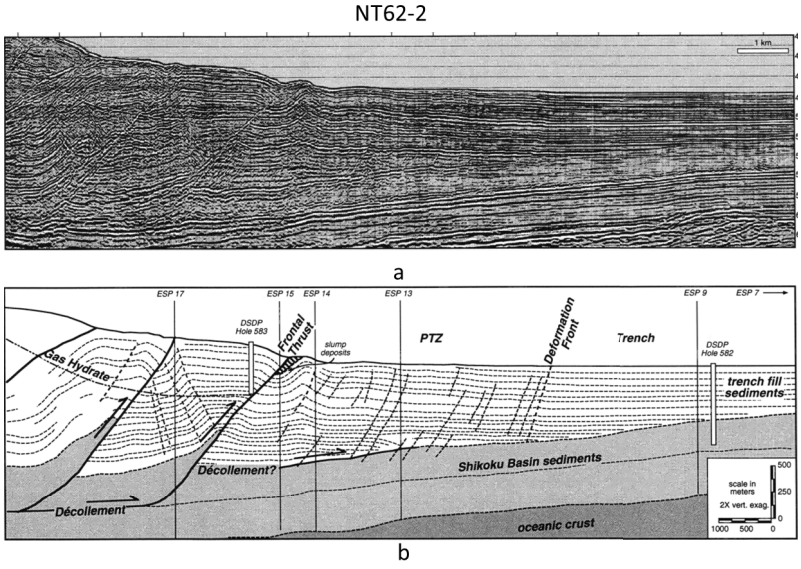

Fig. 5.: Toe of Ashizuri Transect (Morgan et al., 1995)

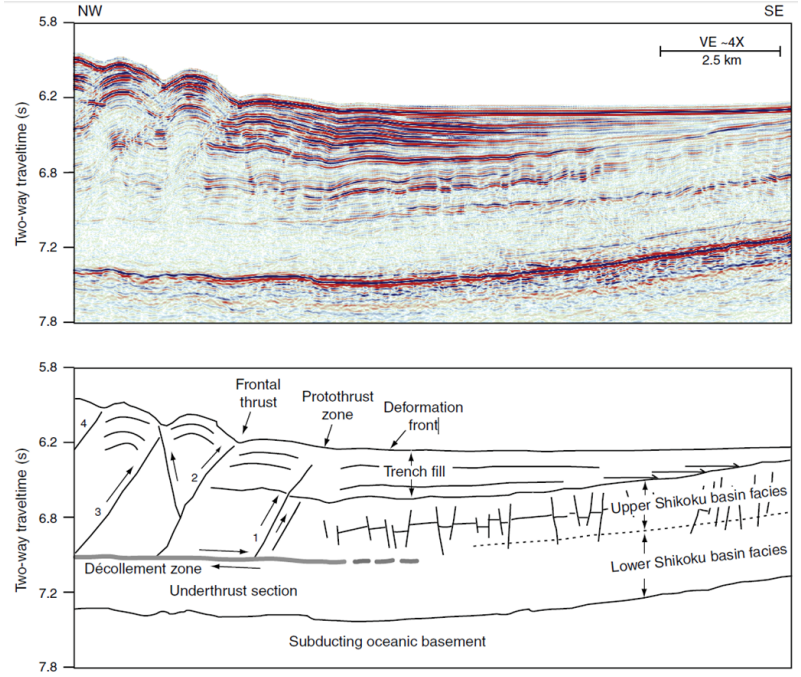

Fig. 6.: Toe of Muroto Transect (Mikada et al, 2005)

The Use of Scaling Theory in Geological Laboratory Models

Olivier Galland[1], Eoghan Holohan[2], Guillaume Dumazer[3]

[1] *Physics of Geological Processes (PGP), University of Oslo, Norway*
[2] *German Research Centre for Geosciences (GFZ-Potsdam), Germany*
[3] *Physics Department, University of Oslo, Norway*
e-mail: *olivier.galland@fys.uio.no*
session: *Methods and Materials*

The main advantage of laboratory modelling, *i.e.* that geological processes are simulated within the limits of a laboratory and the working time of the researcher, at the same time represents the method's biggest problem: the difference in scale between geological systems and the experimental setup in the laboratory can be enormous. It is this scale gap that often leads to scepticism among Earth scientists regarding the applicability of laboratory models.

The geological applicability of laboratory results requires a robust scaling analysis [Hubbert, 1937; Ramberg, 1967]. Nevertheless, there is a lot of confusion among Earth scientists about scaling of laboratory models to geological systems, and first of all about the meaning of "scaling". The main confusion is related to the goals of laboratory models. They are not designed to mimic a given geological system, as many Earth scientists think, but to understand generic processes, either individually or in combination, and to identify or demonstrate physical laws governing these processes. In order to prove that any physical laws identified in laboratory experiments apply to geological systems, these laws should be dimensionless, *i.e.* they are independent of the length scale, time scale, etc... If an established law depends on the observational dimensions, the physical generality fails and the laboratory results cannot be extrapolated to geological systems.

The procedure for establishing dimensionless scaling laws involves two steps: (i) a *dimensional analysis* of the considered physical problem, to identify the dimensionless governing parameters, and (ii) a *comparison of laboratory and geological values of these dimensionless parameters (called similarity)* to test the geological relevance of the experimentally-derived physical laws.

Dimensional analysis

The principles of dimensional analysis are described in detail by *e.g.* Barenblatt [2003]. The approach consists in identifying the dimensionless physical parameters that govern the processes to be addressed.

The first step is to list the n parameters with dimensions that are relevant for the processes to be studied. In mechanical systems, usual dimensions are those of length (L), mass (M) and time (T). From this list of parameters, the experimentalist should separate the governing parameters, *i.e.* those known and controlled, from the output parameters to be measured. In the field of phase transition the notions of 'control parameters' and 'order parameter' are often in use.

The second step is to identify the number k of the governing parameters with independent dimensions. A set of parameters has independent dimensions if their dimensions cannot be expressed as a function of each other's [Barenblatt, 2003]. For instance, the height of a volcanic edifice and the density of the rock have independent dimensions, because the dimension of the density ($[\rho] = ML^{-3}$) cannot be expressed as a function of the dimension of the depth ($[h] = L$) only. In contrast, the rock cohesion ($[C] = ML^{-1}T^{-2}$), the density ($[[\rho] = ML^{-3}$),

the gravity ($[g] = LT^{-2}$) and the height of, *e.g.* a volcanic edifice ([h]=L) do not have independent dimensions, given that the dimension of C is a function of the dimensions of ρ, g and h:

$$\begin{aligned}[C] &= ML^{-1}T^{-2} = [\rho] \times [g] \times [h] \\ &= (ML^{-3}) \times (LT^{-2}) \times (L)\end{aligned} \quad (1)$$

The third step is to calculate the number m of dimensionless parameters that characterise the physical system to be simulated in the experiments. This number is easily calculated by using the Π-theorem (or Buckingham Π-theorem), which is the central theorem in dimensional analysis. It states that "*a physical relationship between some dimensional (generally speaking) quantity and several dimensional governing parameters can be rewritten as a relationship between a dimensionless parameter and several dimensionless products of the governing parameters; the number of dimensionless products is equal to the total number of governing parameters minus the number of governing parameters with independent dimensions*" [Barenblatt, 2003]. This means that the number m of dimensionless parameters to be defined is easily calculated by $m = n - k$.

Once the number of dimensionless parameters $\Pi_{i(1 \leq i \leq m)}$ governing the modelled system is calculated, the next step is to identify each of them by combining the dimensional laboratory parameters. Among the n dimensional parameters, if the model output has a measurable quantity x, one dimensionless output number Π should contain x, and the $m - 1$ other dimensionless numbers can be defined as input parameters.

If the dimensional analysis is relevant, the defined dimensionless numbers should have a physical meaning. A good example is the Reynolds number (Re), which quantifies the relative contributions of inertial forces with respect to viscous forces in a flowing fluid: a critical value (Re_c) of the Reynolds number marks the transition between a laminar flow regime ($Re < Re_c$) and a turbulent flow regime ($Re > Re_c$).

The dimensionless parameters identified during the dimensional analysis represent the foundation for the experimental strategy and the analysis of experimental results. Two different approaches can be adopted, depending on the nature of the model outputs.

If the model output is a measured quantity, the aim of the experimental procedure will be to establish a correlation between the measured dimensionless parameter Π and the dimensionless input parameters Π_i (Figure 1a). The Π-theorem states that the output dimensionless quantity Π can be rewritten as a function of the other $m - 1$ Π-numbers, such as:

$$\Pi = F(\Pi_1, \Pi_2, \ldots, \Pi_{m-1}) \quad (2)$$

The function F is the physical law that governs the simulated processes. This relationship between the dimensionless output and the dimensionless input parameters should dictate the experimental strategy. In order to test the effects of each dimensionless parameter Π_i during an experimental project, the dimensional experimental parameters should be varied such that Π_i is systematically varied, while the others are kept constant. Applied to each Π_i-number, the experimental results will contribute to derive the physical laws that govern the processes to be understood by constraining the function F. If the parameters Π and Π_i are well defined, they are expected to correlate (Figure 1a).

If the model output is not a measured quantity, but contrasting physical behaviours, the aim of the experimental procedure will be different. We already mentioned the turbulent and laminar regime in fluid mechanics. Another example of contrasting behaviour is the formation of dykes or cone sheets in volcanic systems [see abstract by Galland et al., session Volcanism and Volcanotectonics; Galland et al., in revision]. Here the aim will be to vary systematically the values of the m dimensionless parameters Π_i and then to map under which conditions these contrasting physical behaviours occur (Figure 1b). This procedure is equivalent to building a phase diagram, the contrasting physical behaviours being analogue to physical phases.

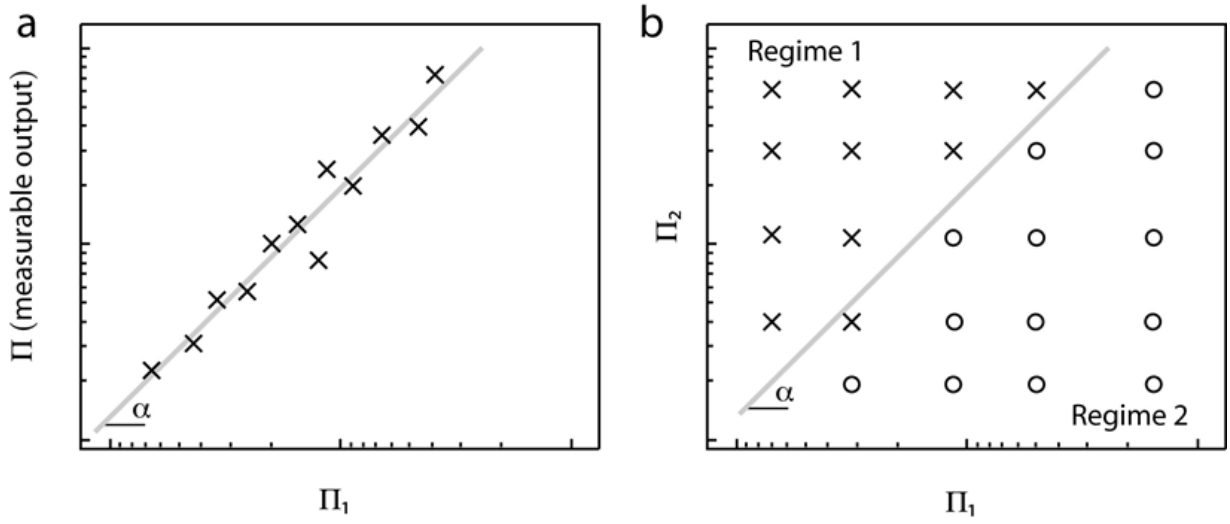

Fig. 1.: Conceptual diagrams illustrating how the nature of the experiment output dictates the analysis of that output in terms of the dimensionless model parameters. a. If the model output is a measured quantity Π, the results will be displayed as a correlation between Π and the input parameters Π_i. b. If the model output is a physical regime, the results will be displayed as a dimensionless phase diagram.

Similarity to geological systems

Following the dimensional analysis and the identification of the Π-numbers, and after obtaining the experimental results that quantify the scaling laws governing the modelled processes, one needs to test the geological relevance and applications of these laws. In other words, we need to test whether the processes simulated in the laboratory are physically similar to the geological processes. This concept of *physically similar phenomena* is central to geological laboratory modelling. *Two systems are considered similar if the values of the dimensionless parameters are identical, even if the values of the governing dimensional parameters differ greatly* [Barenblatt, 2003]. It means that although the scales of the laboratory models are drastically different to the scales of the geological systems they aim to simulate, the laboratory models will be physically similar to their geological equivalents if their respective Π-numbers, as identified in the dimensional analysis, have the same values. Therefore, the experimentalist must compare the values of each Π-number in the laboratory with the values of these numbers in the geological system: if the ranges of values overlap, the two systems are similar, and the experimental results are relevant to the geological system [see abstract by Galland et al., session Volcanism and Volcanotectonics; Galland et al., in revision].

Discussion

A classical approach of laboratory modelling is to use the scaling analysis to justify that the models are representative of their geological prototypes, *i.e.* to use the similarity principle only. Hence, this approach ignores the first part of the scaling procedure, *i.e.* identifying the governing dimensionless parameters to establish the experimental strategy. In most studies, the model results are plotted in dimensional graphs that are scale-dependent, making it very hard to quantitatively compare laboratory results with geological data. Therefore, these studies underuse the fundamental implications of the scaling theory.

Conversely, using the full procedure dictated by the scaling theory offers several crucial advantages:

- the fundamental dimensionless parameters that govern the modelled physical system are identified;

- the list of dimensionless parameters helps to define and focus experimental strategy;
- plotting the model outputs in dimensionless forms reveals the fundamental scale-independent physical laws that govern the modelled processes;
- consequently, it is possible to quantitatively compare laboratory results and geological data in the same dimensionless plots to test the geological relevance of the laboratory results.

References

Barenblatt (2003), Scaling, 171 pp., Cambridge University Press, Cambridge.

Galland et al. (in revision), Toward a unified model for dykes versus cone sheets in volcanic systems, J. Geophys. Res.

Hubbert (1937), Theory of scale models as applied to the study of geologic structures, Geol. Soc. Am. Bull., 48.

Ramberg (1967), Gravity, deformation and the Earth's crust as studied by centrifuge models, 452 pp., Academic Press, New York.

Testing tools for the generation of an unstructured tetrahedral grid on a realistic 3D underground model

Ines Görz[1], Felix Träger[1], Björn Zehner[2], Jeanne Pellerin[3]

[1]*Department of Geophysics and Geoinformatics, TU Bergakademie Freiberg, Gustav-Zeuner-Str. 12, 09599 Freiberg, Germany*
[2]*Bundesanstalt für Geowissenschaften und Rohstoffe, Dienstbereich Berlin, Wilhelmstraße 25-30, 13593 Berlin, Germany*
[3]*IUniversité de Lorraine, GeoRessources UMR7359, CNRS, CREGU, ENSG, 2 rue du doyen Marcel Roubault, TSA 70605, 54518 Vandoeuvre-Lès-Nancy Cedex, France*
e-mail: *IGo@geo.tu-freiberg.de*
session: *Methods and Materials*

Introduction

Numerical simulations of stress field, heat flux and groundwater flow are important for modern investigations of the geological underground performed by geo-consulting and resource exploration companies. However, the simulation results are only meaningful if the geology of the research region is represented adequately.

Realistic underground models are generated with dedicated geomodeling software like Petrel, Move3D, Gocad and Skua, which integrate all available data while respecting geological concepts and the data as geometry and property constraints. The structural models generated by the geomodeling software usually describe the geometry of the subsurface by boundary surfaces. From these surfaces, a boundary representation model can be created (Weiler, 1988; Duvinage et al., 1999). A coherent boundary representation is achieved when the volume of the body is completely confined and partitioned by surfaces without holes and overlaps (Caumon et al., 2004). If the model is to be used for calculations, its volume has to be discretized into cells each of which belongs to one unique geological unit. Depending on the method of computation to be applied, different cell types are used.

Unstructured grids are often used with finite element (FE) based software codes (Schwarzbach et al., 2011, Afanasjew et al., 2013). Unstructured grids consist of an irregular pattern of grid points with neither a pre-defined topology nor fixed cell geometry. Unstructured meshes do not have a regular connectivity, i.e. their vertices do not all have the same number of neighbors. Tetrahedral meshes are the most versatile unstructured meshs, therefore they can represent any geometry. They can be built automatically respecting predefined mesh properties. In this study, we created a structural 3D model with the Paradigm Skua software and tested workflows for generating a tetrahedral unstructured grid suitable for FE simulations on this model.

Skua uses a fully-volume based modeling approach, which interpolates geological horizon surfaces implicitly as iso-surfaces on a tetrahedral mesh, while accounting for faults. The cells of the primary tetrahedral mesh cross horizon boundaries, therefore the resulting structural model has to be transformed into a boundary representation and then be re-meshed by a tetrahedral grid which respects all geological boundaries.

The first step towards creating a tetrahedral mesh consists of generating and combining loose surfaces to make a boundary representation. Since Gocad/Skua creates and edits the triangular surfaces (TSurfs) independently of each other, the nodes of two surfaces at one surface contact

are usually not identical.

Each workflow has to generate triangulated surfaces that have the same geometry along their lines of intersection, i.e. they must have identical vertices and segments. The tetrahedrons should have a suitable quality, which means the aspect ratio should not be too great because numerical instabilities can occur in such tetrahedrons. Mesh quality definition completely depends on the application. Typically a set of quality criteria on the size, shape, and orientation is taken into account at the mesh generation step.

In order to formulate boundary conditions, certain points or lines are often required to be part of the mesh. The workflow has to be able to add these objects as constraints to the tessellation.

If, for example, a geophysical measurement is simulated, the mesh resolution also needs to be adapted to the measurement method. In particular, the mesh has to be refined in the vicinity of the source and receivers to avoid aberrations across the whole modeling domain.

Test case "relay ramp"

We used the 3D structural model of a normal fault relay ramp to test the tessellation workflows.

The structure consists of two overlapping fault segments connected by a soft linkage zone that transfers displacement from one fault segment to the other. The model includes three stratigraphic horizons displaced along the two normal faults, both of which terminate in the modeling domain (fig. 1). Generation of a tetrahedral mesh in this model is challenging since:

- the horizon-fault contact lines cut one another at narrow angles, such that flat acute-angled tetrahedrons are generated;
- the two faults end inside the model;
- the triangulation of the fault surfaces has to respect vertices of the fault-contact lines, which usually cross one another, such that a constrained triangulation including crossing lines is necessary in order to create a conformal triangulation.

Workflows

Skua Finite Element Mesh Constructor

Gocad/Skua provides a commercial module for constructing tetrahedral meshes, the Finite Element Mesh Constructor (FEMC). This tool works with a Weiler boundary representation (Weiler, 1988), the so-called Model3D, which can be transformed into a tetrahedral mesh using the FEMC. This module works fully automatically: only the number of tetrahedrons has to be specified. The tetrahedral mesh consists of parts representing the geological units, and the vertices at the boundary of each part are duplicated. The FEMC in combination with Skua generates an overall good mesh quality in many cases. However, tessellation of the relay ramp model failed during re-meshing the surfaces.

Gmsh and TetGen via Skua plugin CompGeom

This workflow combines Skua and Gocad with the opensource softwares Gmsh (Geuzaine and Remacle, 2009) and TetGen (Si, 2011). In order to manipulate Skua and Gocad objects and to communicate with Gmsh and TetGen, Gocad/Skua was extended by implementing the CompGeom plugin (Zehner, 2011). First, a framework of all surface outlines and contacts has to be extracted in Skua. In order to smooth the curves or to get a regular spacing of the curve nodes, the curves can be resampled with a cubic spline function which conserves the original shape of the objects. The line framework of each surface is exported to Gmsh. Gmsh creates a triangulation incorporating all nodes of the framework. The resulting triangulated surfaces are read back to Skua and the surfaces are transformed back to their 3D geometry. In this way, all surfaces have to be re-meshed until a watertight boundary representation is obtained. During this re-meshing process, further lines and points can be added, so that they are part of the triangulation. This option can be used to provide the necessary geometry for defining boundary conditions at the surface or to enforce local refinements of the mesh. Next, the

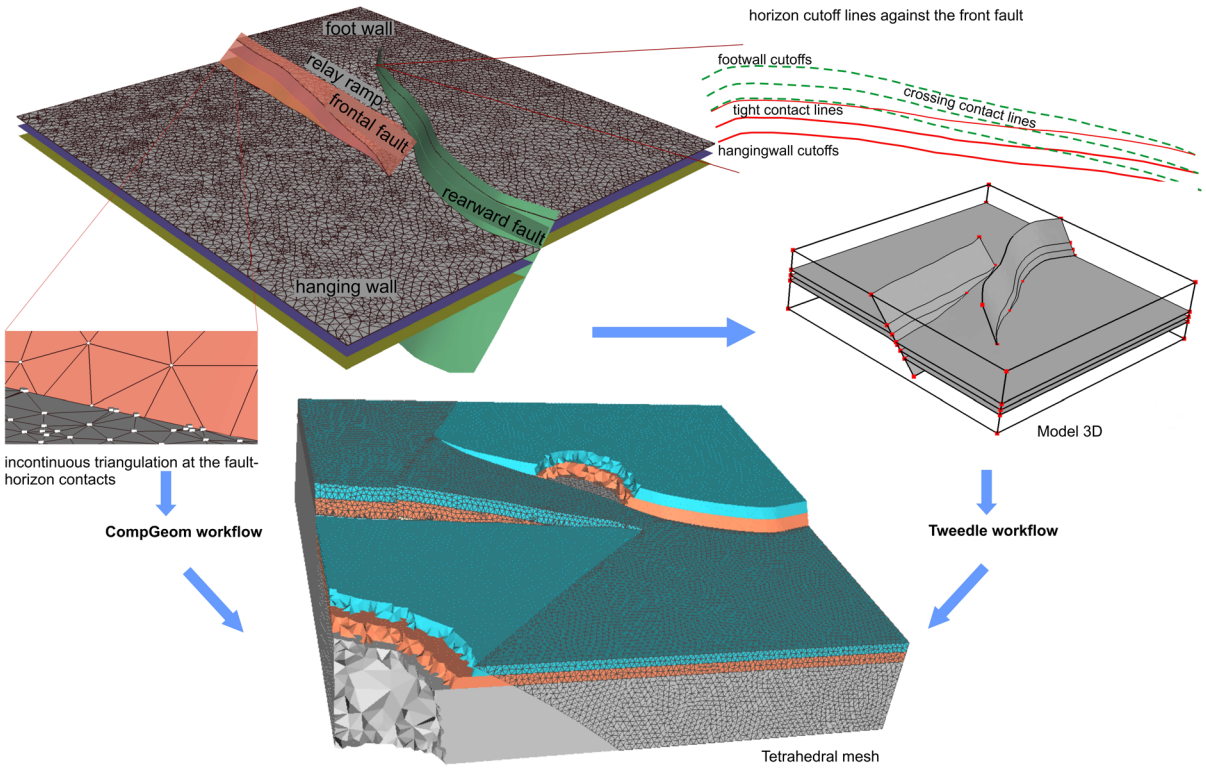

Fig. 1.: 3D model of a relay ramp consisting of triangulated boundary surfaces and a tetrahedral mesh.

finite element mesh can be produced. To accomplish this, all surfaces of the model are exported to a TetGen input file. This file contains duplicate but identical vertices as one global point. If the model is partitioned by internal surfaces, TetGen can recognize this, and each tetrahedron is assigned a number indicating the partition it belongs to. This number can be later used for setting material parameters. The TetGen output can be used as input for the simulation software or be imported back into Gocad/Skua for quality control and further processing.

Graphite Voronoi based re-meshing via the Skua plugin Tweedle and TetGen

When using the surface structural model built by Skua, it is necessary to re-mesh these surfaces. This means improving their quality and adapting triangle sizes. We use the surface re-meshing method recently proposed by Pellerin et al. (2014). This method, specifically developed for geological models, is based on the notion of Centroidal Voronoi Diagrams (Du et al. 1999). The two main steps of the method are (1) to optimize the positions of the vertices of the output mesh and (2) to consider a 3D subdivision of the model, determined from these points, to build the triangles of the output mesh. The method is automatic, it re-meshes all surfaces and contact lines at the same time with a controlled number of triangles, and the output mesh triangle quality does not depend on the input mesh quality. This mehtod is implemented in a plugin of the research modeling software Graphite (`http://alice.loria.fr/index.php?option=com_content&view=article&id=22`) that is interfaced in Gocad through the plugin Tweedle Pellerin et al. (2010). The resulting set of surfaces was exported to TetGen.

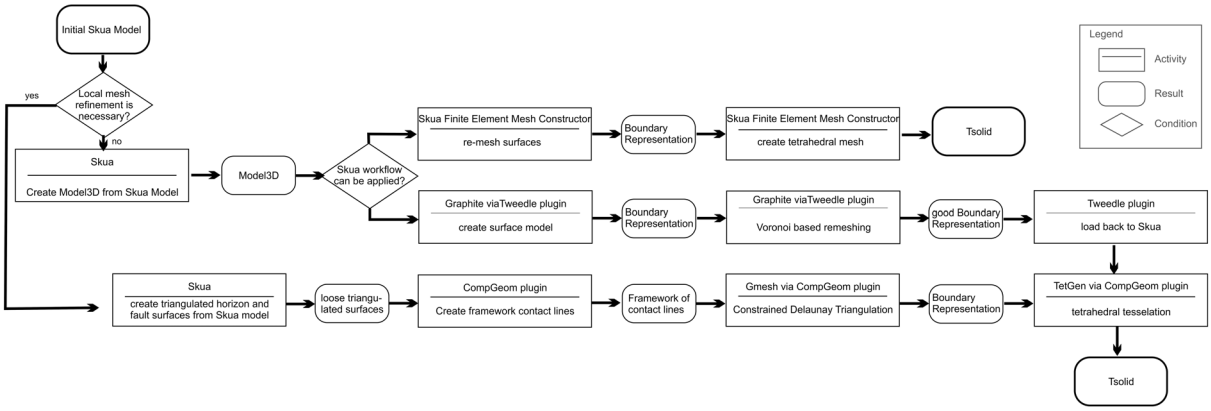

Fig. 2.: Workflows for generating a 3D tetrahedral grid.

Results

While preparing a 3D Skua model for a FE simulation on an unstructured tetrahedral grid, the major part of the work consists in generating a continuous triangulation of the geological boundary surfaces in a good quality (fig. 2). The meshing software has to handle crossing contact lines and non-manifold surfaces and to provide a good mesh quality for running a numerically stable process simulation.

The tools developed by Pellerin et al. (2014) permit to re-mesh the surfaces of our boundary representation model with triangles as equilateral as possible in a short time of approximately 30 minutes. The size of the triangulation can be specified by setting the desired number of vertices in the final mesh. If surface contact lines are situated very tight up against one another, the model can be simplified automatically by setting a merging distance. In the current version, the mesh cannot yet be locally refined.

Creating the boundary representation with the CompGeom plugin requires much more working time - in the case of our relay ramp model approx. 2 days. However, the CompGeom plugin in combination with Gmsh allows the mesh geometry and quality to be controlled in detail. The user can specify the distance of the triangle nodes along the contact lines, add lines and points to the triangulation and refine the triangulation locally.

Conclusions

Currently the use of external software is often necessary if a Skua model has to be prepared for a FE simulation. In this study, we tested the Tweedle and CompGeom research plugins, which are both well suited to performing this task. Tweedle is comfortable to handle and a very fast tool, which automatically re-meshs a boundary representation. CompGeom allows for very detailed control over the triangulation, but requires a lot of manual work. Working with both plugins, the surface meshes obtained had to be reworked by hand in order to generate a perfect triangulation which can be used for the generation of an unstructured tetrahedral mesh.

References

Afanasjew M., Börner R.-U., Eiermann M., Ernst O., Spitzer K. (2013): Efficient Three-Dimensional Time Domain TEM Simulation Using Finite Elements, a Nonlocal Boundary Condition, Multigrid, and Rational Krylov Subspace Methods. Expanded Abstracts, 5th International Symposium on Three-Dimensional Electromagnetics, May 7 – 9, 2013, Sapporo, Japan, 4p.

Caumon G.,Lepage F., Sord C.H., Mallet J.-L. (2004): Building an Editing a Sealed Geological Model. Mathematical Geology, 36/4, 405-424. Du Q., Faber V., Gunzburger M. (1999):

Centroidal Voronoi Tesselations: Applications and Algorithms. SIAM Review 41/4, 637-676.

Duvinage I., Mallet J. L., Dulac J. C. (1999): Extracting information from faulted horizon boundaries for building and updating of a 3D model. Annual Meeting Expanded Abstracts, American Association of Petroleum Geologists, A35.

Geuzaine C., Remacle J.-F. (2009): Gmsh: a Three-Dimensional Finite Element Mesh Generator with Built-in Pre- and Post-Processing Facilities. International Journal for Numerical Methods in Engineering 79, 1309 – 1331.

Moyen R. (2005): Throw modeling on unstructured Objects. 25th Gocad Meeting, Nancy, 19pp.

Muron P. (2005): Handling faults in 3D structural restoration. 25th Gocad Meeting, Nancy, 15pp.

Schwarzbach C., Börner R.-U., Spitzer K. (2011): Three-dimensional adaptive higher order finite element simulation for geo-electromagnetics—a marine CSEM example. Geophys. J. Int., 187, 63-74.

Pellerin J., Levy B., Caumon G. (2010): Advanced geometry processing in Gocad using Graphite. 30th Gocad Meeting, Nancy, 8 pp.

Pellerin J., Levy B., Caumon G., Botella A. (2014): Automatic surface remeshing of 3D structural models at specified resolution: A method based on Voronoi diagrams. Computers and Geosciences 62, 103-116.

Si H. (2011): TetGen, A Quality Tetrahedral Mesh Generator and a 3D Delaunay Triangulator. http://wias-berlin.de/software/tetgen//, last time visited July 2014.

Weiler K., (1988): The radial edge structure: A topological representation for non-manifold geometric boundary modeling. In Wozny M., McLaughlin H., Encarna, eds., Geometric modeling for CAD application. Elsevier Amsterdam, 3–36.

Zehner B. (2011): Constructing Geometric Models of the Subsurface for Finite Element Simulation. Conference of the International Association of Mathematical Geosciences (IAMG 2011), Salzburg, Austria, 5th-9th September 2011, doi:10.5242/iamg.2011.0069.

Flanking structures – New insights from analogue models

C. J. S. Gomes[1], Rodrigues, B. A.[1], Endo, I.[1]

[1] *Departamento de Geologia, Universidade Federal de Ouro Preto, Morro do Cruzeiro s/no; 35.400-000 Ouro Preto, Minas Gerais (Brasil)*
e-mail: *caroline.janette@gmail.com*
session: *Methods and Materials*

Introduction

Flanking folds are deflections of planar or linear fabric elements in the vicinity of crosscutting objects (Grasemann & Stüwe 2001; Passchier 2001) that occur in a wide range of tectonic environments and rock types. These structures challenged geologists because of their common counter-intuitive behavior as they may show shear sense opposite to the effect of fault drag. Thus flanking folds, collectively termed flanking structures by Passchier (2001), must be used with caution as shear sense indicators.

Several explanations have been proposed to explain the origin of the flanking folds in shear zones, such as the reduction of the flow velocity alongside veins, dykes or faults, the type of ductile flow and the initial orientation of the crosscutting element (e.g. Passchier 2001; Grasemann & Stüwe 2001; Grasemann et al. 2003; Wiesmayr & Grasemann 2005).

Numerous numerical modeling studies concerning the kinematics of flanking structures have been presented but analogue models are not common. Hudleston, in 1989, was the first author who generated flanking structures in analogue experiments. He used plasticene in simple shear and showed that the progressive rotation of an extensional fracture causes the formation of folds not by slip along the fracture margins but passively by a local contraction.

Odonne (1990) employed horizontal paraffin wax layers to analyse the deformation intensity around a fault, by uniaxial compression. He concluded that a fracture locally disturbs stress and deformation fields producing a non-coaxial strain history.

Exner et al. (2004) used silicone, a linear viscous material, in a ring shear rig, to test and extend previous numerical models of type-s flanking folds to higher shear strains. The authors showed that both offset and deflection of type-s flanking folds along a central discontinuity document a local contraction of the planar fabric elements parallel to the shear zone boundary. In addition, they suggest that, as the crosscutting element itself co-rotates, in principle, at high shear strain all flanking structures may evolve to type-s flanking folds.

The aim of this work is to present new analogue models of flanking folds above a single strike-slip fault using a linear viscous silicone of low viscosity and compare them with those presented by Exner et al. (2003).

Model set up and procedure

Seven models were built and deformed in a rectangular box, 33 cm long, 20 cm wide and 1.5 cm deep. An electric motor displaced one half of the box horizontally, producing a sinistral fault slip at shear strain rate of 6.9×10^{-3} s^{-1}(2 cm/h). As the shear zones in our experiments were only 6 cm large, the lateral boundaries had no effect on deformation. Figure 1 shows the set-up of one of the seven experiments, with the five horizontal lines representing marker lines (the planar fabric elements), and a thin metal plate the crosscutting element. Following Exner et al. (2004), we used liquid soap as a lubricant along the metal plate

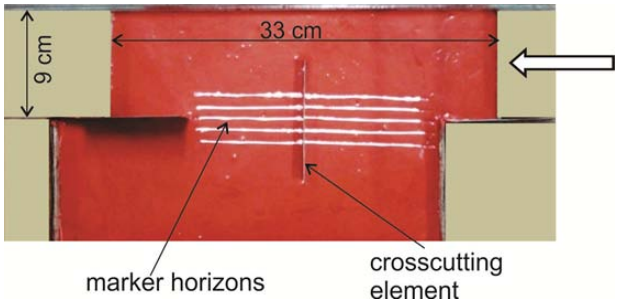

Fig. 1.: The initial set-up of our experiments shown by model CIS90. Arrow shows the direction of the movement.

to simulate slip along an active fault.

The silicone used as a ductile matrix was a mixture between mastic silicone rebondissant 36 (from E^{ts}E. H. Roberts et Cie, CRC) and alcohol, with a resulting viscosity $\mu = 1.7 \times 10^4$ Pa s, at 21 °C. The models were deformed by a total shear strain of $\gamma = 1.3$, that corresponds to 8 cm of linear dislocation.

Based on Grasemann et al. (2003) and Exner et al. (2004), we used seven different initial angles ϕ of the crosscutting element to the shear zone boundary ($\phi = 15°$, 30°, 70°, 90°, 110°, 150° e 165°). The experiments were named according to their angle ϕ: CIS15, CIS30, CIS70, CIS90, CIS110, CIS 150 and CIS165, and to facilitate we used the terminology provided by Grasemann et al. (2003) for the experimental result descriptions. To ensure reproducibility we performed each experiment twice.

Results

The line drawings of figure 2 summarize our experiments. Models are shown prior to and at final stage of deformation, followed by an interpretative sketch and the flanking structure classification.

The most interesting feature of our experiments is the markedly different amount of offsets of the marker lines that led to thickening and thinning of the silicone at crosscutting element terminations. The offsets varied along the crosscutting element (sense and magnitude) both among the five marker lines of one experiment and among the seven experiments. The deflections of the marker-lines, adjacent to the crosscutting element, were also heterogeneous as they vary over the length of the crosscutting element. In addition, if considering only the upper marker lines, all experiments except the models CIS15 and 30 show contractional deflection. However, analyzing the central marker line (accordingly to Grasemann et al. 2003) it is notable that offsets were extensional in models CIS15, 70, 90, 110 and 165 and despicable in the models CIS 30 and 150. At final deformation, we classified the instantaneous flanking structures as extensional normal a-type, extensional reverse a-type, shear band and n-type flanking folds (Fig. 2).

Discussion/Conclusions

The deviation of the square grid, marked on an additional experiment set up without the crosscutting element, showed the silicone flow trajectory (Fig. 3). This trajectory suggests that the introduction of a discontinuity acted as an obstacle modifying the flow field. As thickening and thinning of silicone at crosscutting terminations are consistent with sinistral simple shear, the modelled flanking folds should have formed by perturbation strain. We suggest that this deformation occurred in our experiments because of the relative low viscosity of the silicone.

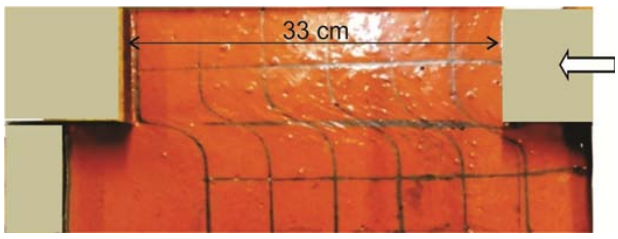

Fig. 3.: The silicone flow trajectory after the sinistral simple shear in an additional model set up with an initial square grid and without the crosscutting discontinuity. Arrow indicates the direction of the movement.

In the literature, natural examples of flanking folds, comparable to the model results, are

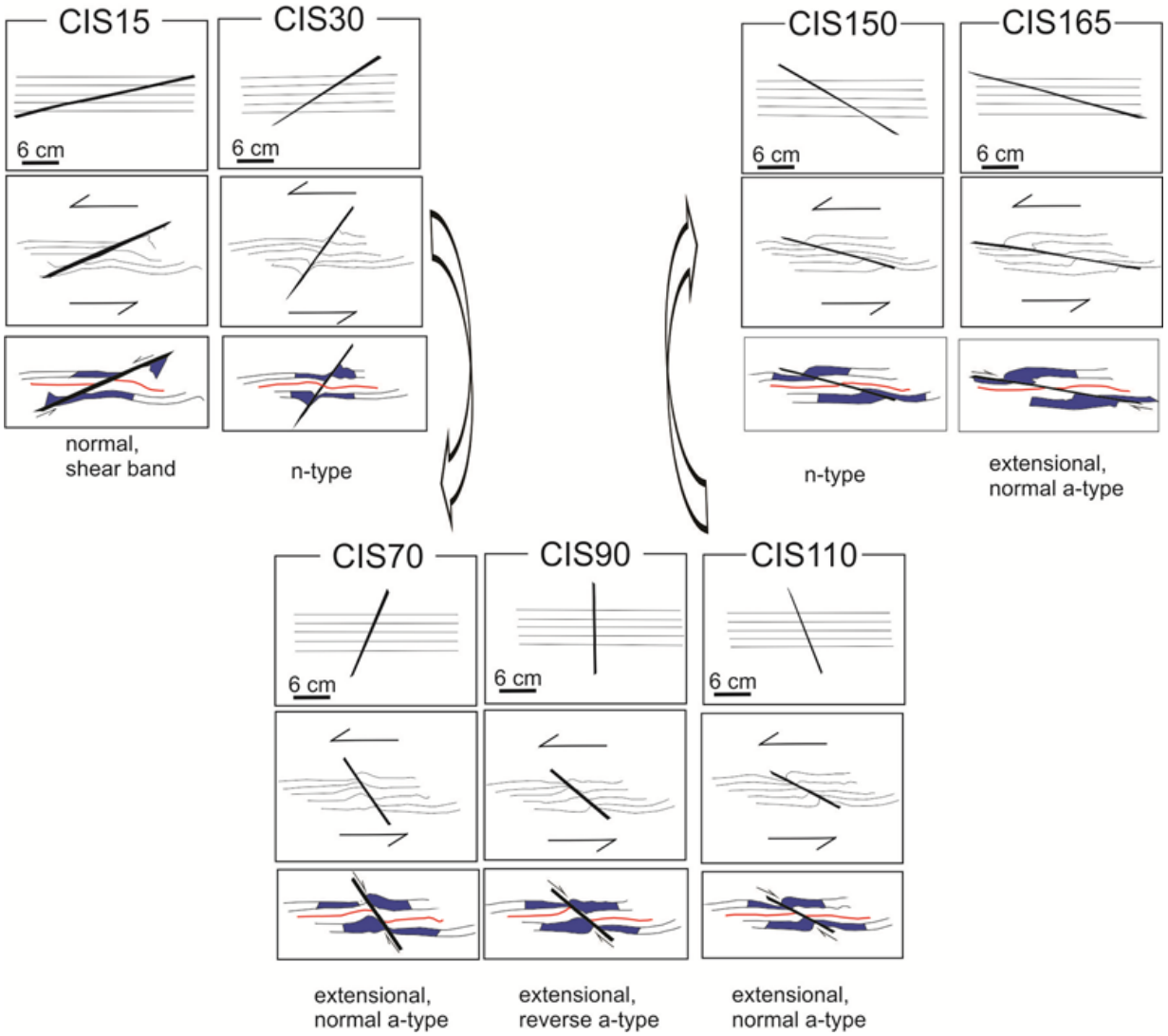

Fig. 2.: Line drawings of the seven analogue experiments with initial angle $\phi = 15°$ (CIS15), 30° (CIS30), 70° (CIS70), 90° (CIS90), 110° (CIS110), 150° (CIS150) and 165° (CIS165) to the shear zone boundary. Each experiment is shown at $\gamma = 0$ and at final $\gamma = 1.3$, without and with interpretation of instantaneous flanking fold type. Note thickening and thinning of the silicone at opposite terminations of the crosscutting element.

common in medium to high grade metamorphic rocks. Thus, our experiments suggest that the flow characteristics constitute an additional factor controlling flanking fold geometries.

Acknowlegments

We acknowledge Fundação de Amparo à Pesquisa do Estado de Minas Gerais (Fapemig) (CRA-APQ-01672-11 and CRA-PPM-00531-13) for financial support.

References

Exner U., Mancktelow N.S., Grasemann B. 2004. Progressive development of s-type flanking folds in simple shear. Journal of Structural Geology 26: 2191-2201.

Grasemann, B., Stüwe, K. 2001. The development of flanking folds during simple shear and

their use as kinematic indicators. Journal of Structural Geology 23: 715-724.

Grasemann B., Stüwe K., Vannay J.-C. 2003. Sense and non-sense of shear in flanking structures. Journal of Structural Geology 25: 19-34.

Hudleston P. 1989. The association of folds and veins in shear zones. Journal of Structural Geology 11: 949-957.

Odonne, F. 1990. The control of deformation intensity around a fault: natural and experimental examples. Journal of Structural Geology, 12: 911–921.

Passchier C.W. 2001. Flanking structures. Journal Structural Geology 23, 951–962.

Wiesmayr G. & Grasemann B. 2005. Sense and non-sense of shear in flanking structures with layer-parallel shortening: implications for fault-related folds. Journal of Structural Geology 27: 249-264.

The Ribbon Tool

J. Großmann[1], J. F. Ellis [1], H. Broichhausen[1]

[1] *Midland Valley Exploration, 2 West Regent Street, Glasgow G2 1RW, United Kingdom*
e-mail: *johannes@mve.com*
session: *Methods and Materials*

3D geological modelling may inherit a high level of uncertainty, being representations of the interpreters understanding of reality. As predictions made always rely on assumptions all the results a geologist gains from geological models comprise interpretational problems that have to be faced by building more constrained models. One approach for constraining and validating a given 3D model is to use the intrinsic rules in a predictive way during the model building process. This way, geometric objects like 3D lines and surfaces can be used to aid the model building process.

Structural traces such as outcrop traces intersecting with elevation contours allow the geologist to predict the geometry of a horizon in the subsurface (Groshong, 1999). Transferring these 2D or 2.5D horizons into 3D is laborious work and a lot of uncertainty may remain. A direct use of 3D lines formed from the intersection of structural traces on a 3D topography represents an alternative method.

Software often provides the possibility of creating 3D surfaces based on 3D line data, by extending a line into the third dimension according to a certain dip and dip azimuth. This method produces simple geometries and can provide reasonable results for subsurface models. However, Midland Valley's Move^{TM} software improves on this method with the 3D dip domain construction in the Ribbon Tool. It provides a distinctive approach which allows the creation of surfaces with varying orientation along its length (Fig. 1). It can be used as a predictive tool in geological models with complex geometries.

In Move, Ribbon construction is based on the three-point approach which involves using three points with known x, y, z coordinates and calculating the orientation (azimuth and dip) of a planar triangle fitting the three points. The reliability of the computation depends on the number of points selected and on their sample spacing along the line. Developed on the method of Fernandez (2004), where the mean principle orientation is calculated on a radial bias function, the algorithm now calculates the mean principal orientation of each triangle created for every three points along the line. The Ribbon construction in Move 2014 defines an additional search window interval based on a set distance from the center point of a triangle. It then averages the mean principal orientation of the included triangles and produces several 3D dip domains along the line (Fig. 2). These are projected as sticks in 3D and can be displayed and created as coherent Ribbon surfaces (Fig. 3, right).

Working with the mean principal orientations of the defined dip domains provides a statistical control towards the shape and strength of the created surface. This information is illustrated in a Fisher plot and classified according to the cluster/girdle classification after Woodcock (1977) (Fig. 3, left). A low K-value represents girdle and a high K-values represents cluster shape mean principal orientations of the dip domains. The M-value is a measure of the statistical strength of the mean principal orientations.

It is important to understand that Ribbon surfaces created on the basis of 3D line data formed from the intersection of geological surfaces are merely a statistical approach and cannot always

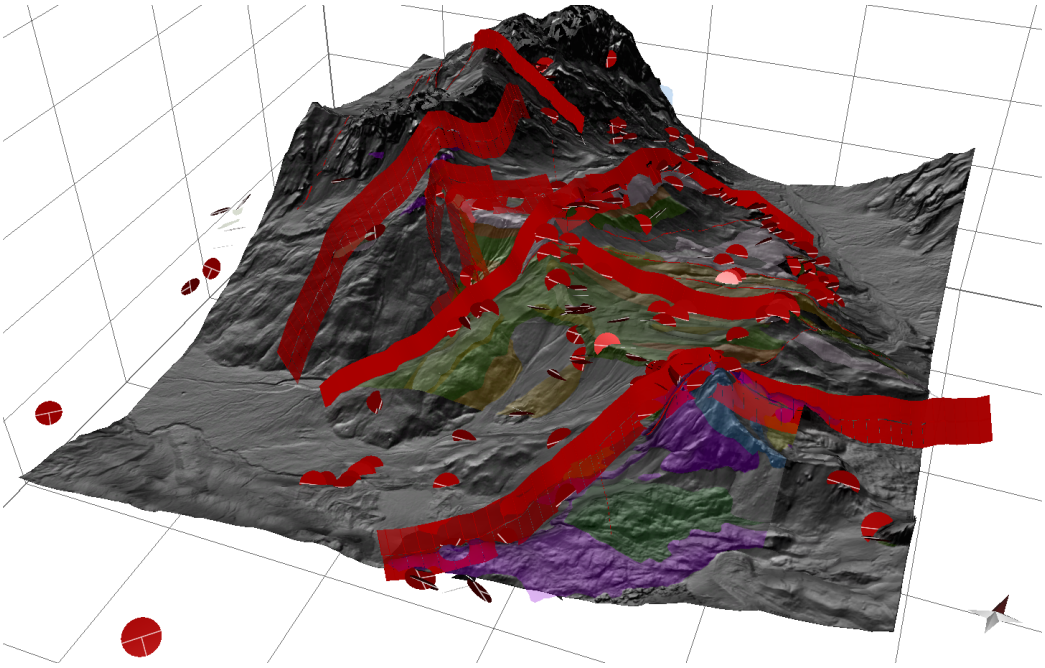

(a)

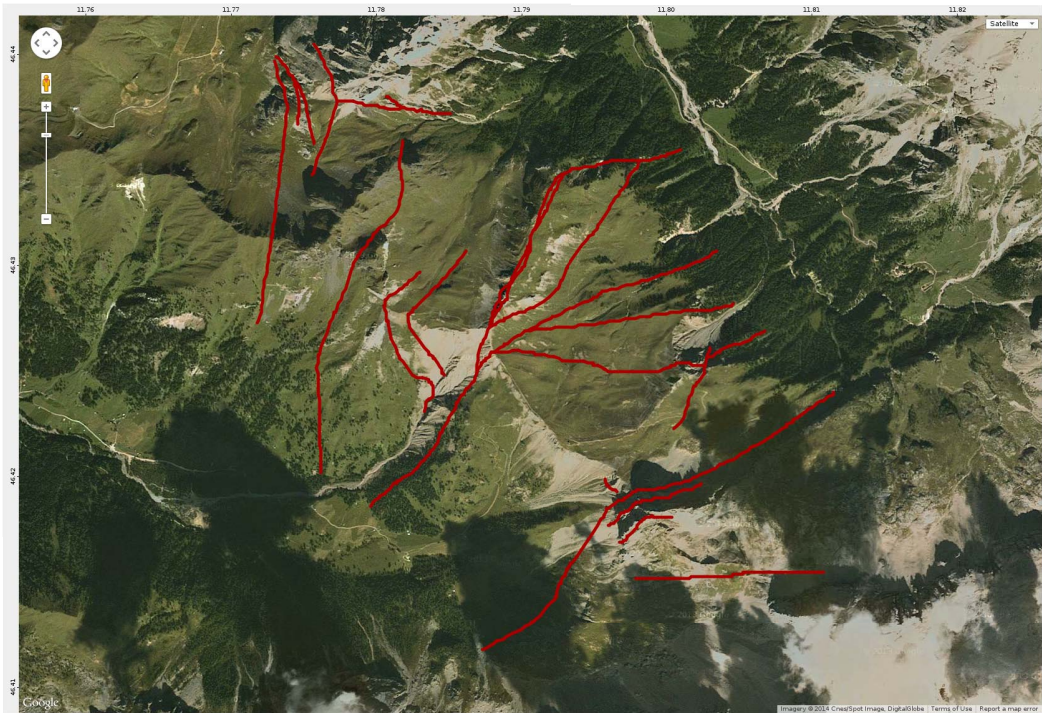

(b)

Fig. 1.: (a) - oblique view of the Digital Elevation Model (DEM) and fault surfaces constructed using the Ribbon tool in Move software, disks represent dips for the various lithologies shown by coloured polygons. (b) - map view of fault traces overlain on Google Satellite image. Data was collected as part of the Innsbruck University Summer School of Alpine Research, from Valle San Nicolò in the Sella Massif, Dolomites Northern Italy. The stratigraphy covers the Dolomites through early rifting and Eoalpine thermotectonics to Neogene indentation.

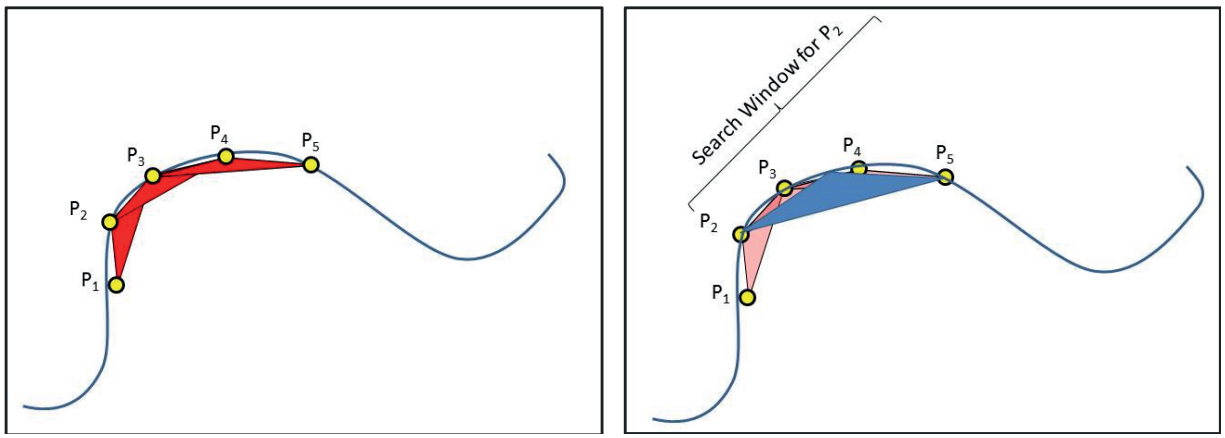

Fig. 2.: Simple representation of a line in space, yellow points (P1-P5) are used in the calculation of dip and dip azimuth. Left - red triangles have been created from every three points. Right - the blue triangle has been created from an average measurement within the selected search window.

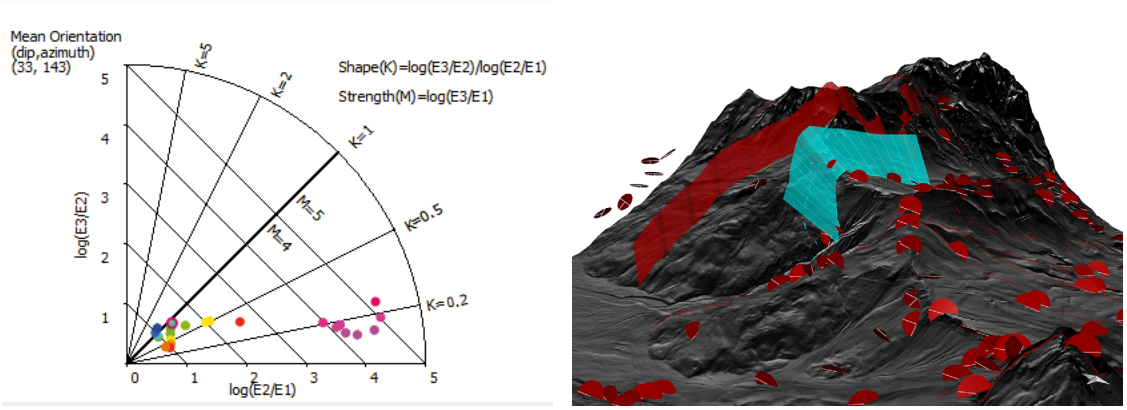

(a) (b)

Fig. 3.: (a) - Fisher plot illustrating the mean principal orientation of dip domains classified after Woodcock (1977). (b) - example of constructed ribbons based on line data on a 3D topography.

constrain the shape and orientation of 3D surfaces in a geologically reasonable way. It is therefore essential for the user to already have a distinct idea of the major geological structure e.g. provided by field orientation data, before starting the Ribbon creation process.

The case studies presented (e.g. Fig. 1. and Fig. 4.) address the practical application of the Ribbon construction as a very efficient method to create 3D surfaces based on dip domains calculated from geological line structures. Although all case study examples presented here demonstrate the use of the tool from surface data, this method can be used in the subsurface on any line with a 3D geometry.

References

Woodcock, N.H. (1977). Specification of fabric shapes using an Eigenvalue method. Bull. geol. Soc. Am. 88, 1231-1236 (47, 48, 49).

Woodcock, N.H. & Naylor, M.A. (1983). Randomness testing in three-dimensional orientation data. J. Struct. Geol. 5, 539-548 (48,49).

Groshong Jr., R.H. (1999). 3D Structural Geology: a Practical Guide to Surface and Subsurface Map Interpretation. Springer Verlag, Berlin.

Fernandez, O., Munoz, J. A., Arbues, P., Falivene, O., Marzo, M. (2004). 3-D reconstruction of geological surfaces: an example of growth strata and turbidite systems from the Ainsa basin (Pyrenees, Spain). AAPG Bulletin, 88, n.8, 1049-1068.

Fernandez, O. (2005). Obtaining and evaluating strike and dip measurements from 3D georeferenced data. Jour. of Structural Geology, 27, p855-858.

Ellis, J., Mannino, I., Johnston, J., Feliks, M.E.J., Younger, P.L. and Vaughan, A.P.M. (2014). Shiremoor Geothermal Heat Project: reducing uncertainty around fault geometry and permeability using MoveTM for structural model building and stress analysis. European Geosciences Union General Assembly 2014, Vienna, 27th April–2nd May 2014. EGU2014-15069.

Acknowledgements

Fig. 1 and 3. “Regione del Veneto – L. R. n. 28/76 – Formazione della Carta Tecnica Regionale” and” Autonome Provinz Bozen – Sud Tirol – Amt fur raumbezogene und statische Informatik/Provincia Autonoma di Bolzano – Alto Adige – Ufficio Informatica geografica e statistica” is acknowledged for the contribution of the DEM.

Figure 4. data curtsey of Cluff Geothermal.

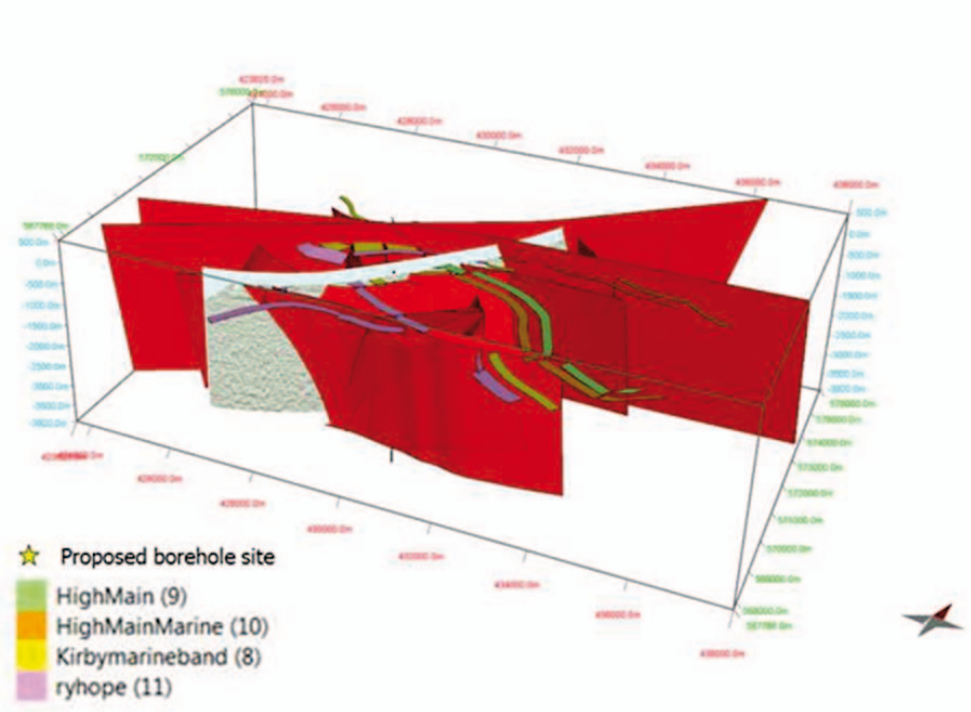

(a)

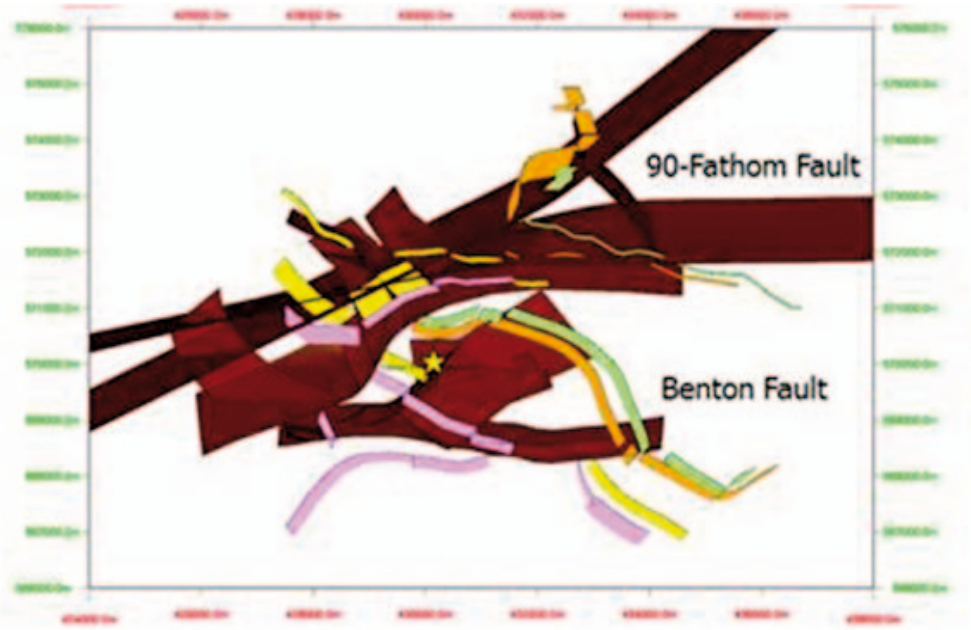

(b)

Fig. 4.: Coal seams construed using surface mapping data and the Ribbon Tool where used to define fault locations and offsets. Oblique (a) and Map (b) view of faults. Fault colour saturation varies with lighting direction (Ellis et al. 2014).

A new method to study the energy budget of rock fragmentation

Øystein Thordén Haug[1], Matthias Rosenau[1], Zahra Amirzada[1], Karen Leever[1], Onno Oncken[1]

[1] *GFZ German Research Centre for Geosciences, Helmholtz Centre Potsdam, Telegrafenberg, D-14473 Potsdam, Germany.*
e-mail: *thorden@gfz-potsdam.de*
session: *Methods and Materials*

Introduction

Fragmentation is a process occurring in several natural systems, e.g. gravitational rock movement [Wang and Tonnon (2010); Locat et al. (2006)]. Despite being a common process, little is known about what governs fragmentation and how it affects the energy of the system. For instance in gravitational rock movements, it is still debated whether fragmentation acts as an energy source [Davies and McSavaney (2009)] or an energy sink [Crosta et al. (2007)]. Our lack of understanding is mainly due to the lack of observations, i.e. the process of fragmentation cannot be quantitatively observed in progress in nature. To overcome this limitation, we have developed a new method where the fragmentation of a new rock analogue material is studied in a controlled laboratory environment. The material strength is scaled to natural rocks and it behaves in a brittle manner (Figure 1a). It is, therefore, ideal for the study of fragmentation under controlled laboratory conditions

Analogue Material

The material is produced by mixing well sorted fluvial sand (average grain size $\sim 300\mu m$) with 2 wt% gypsum powder, while dry. Then, $\sim$10 wt% water is added to the mixture and thoroughly stirred, until a homogeneous material is achieved. The material is left to harden for 2 days. The material properties have been determined by triaxial tests and ring shear tests. The tests show that the primary strength of the material (i.e. its cohesion) can be controlled by the amount of gypsum added to the mixture (Figure 1b). However, the other frictional properties (static friction coefficient, dynamic friction coefficient) remain similar to that of the sand.

Experimental setup

Fragmentation of a sample is induced by impacting on a horizontal plane after being accelerated down a 1 meter slope of 45°. A sketch of the experimental setup is given in Figure 2. The experiments are monitored by two digital optical cameras: one that captures the kinematics of the models at a frequency of 50 Hz, and one that takes a high resolution still image of the final deposits. This ensures both good temporal and spatial resolution. Quantitative measures from the experiments are extracted from the images by binarizing them, i.e. setting all the fragments to 1 and setting everything else to 0.

The energy consumed by fractures is most often characterized by the production of new surface area. Information of the new surface area created in the fragmentation can be measured from the fragment size distribution (FSD). However, to measure the FSD is tedious and difficult. Observations of the FSD (Figure 3), suggests

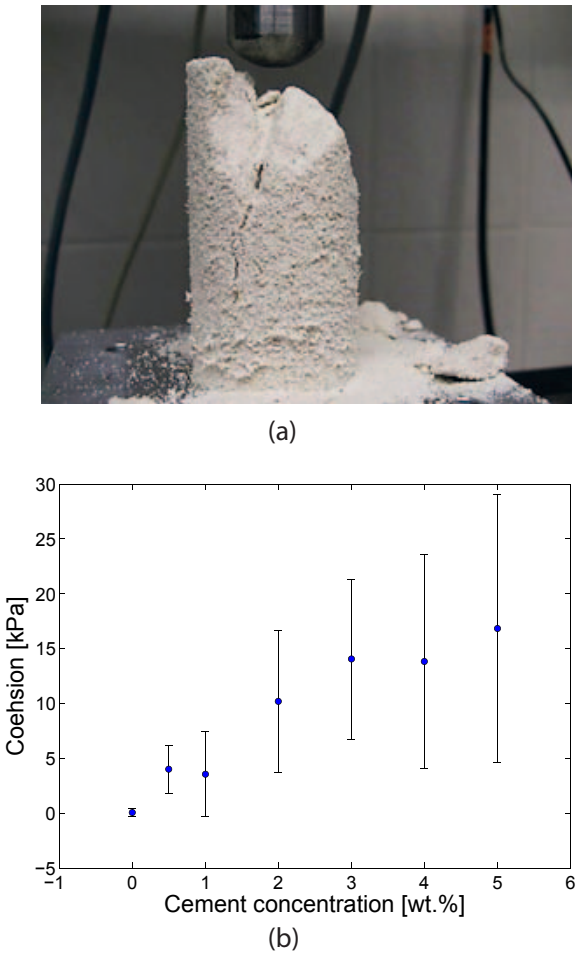

Fig. 1.: Picture of the material after deformation. The material behaves in a brittle manner. (b) The cohesion of the material is controlled by the amount of gypsum powder added to the mixture.

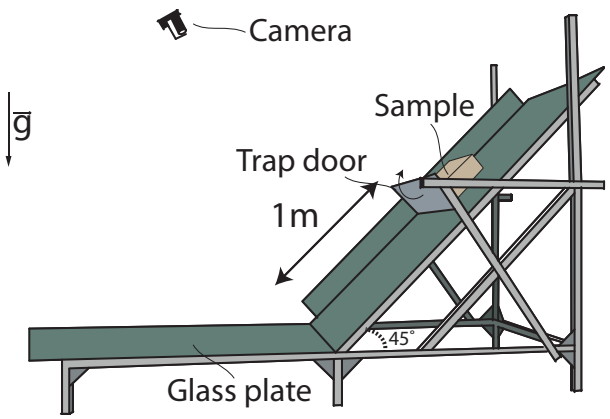

Fig. 2.: Sketch of experimental setup

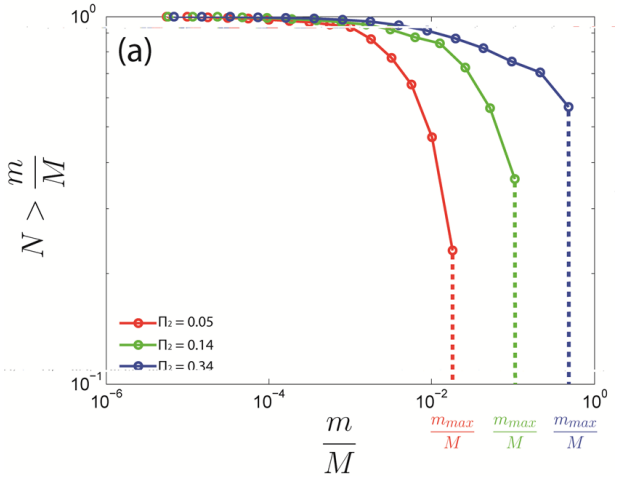

Fig. 3.: Three fragment size distribution for different degrees of fragmentation. The parameter m_{max}/M is observed to act as both a scale parameter and a shape parameter for the distributions.

that the parameter m_{max}/M acts as both a scale parameter and a shape parameter for the FSD, suggesting that we can characterize the fragmentation process with m_{max}/M.

References

Crosta, G. B., Frattini, P., Fusi, N., Feb. 2007. Fragmentation in the Val Pola rock avalanche, Italian Alps. Journal of Geophysical Research 112, F01006.

Davies, T. R., McSaveney, M. J., 2009. The role of rock fragmentation in the motion of large landslides. Engineering Geology 109 (1-2), 67-79.

Locat, P., Couture, R., Leroueil, S., Locat, J., Jaboyedo, M., 2006. Fragmentation energy in rock avalanches. Canadian Geotechnical Journal 43 (8), 830-851.

Wang, Y., Tonon, F., Jul. 2010. Discrete Element Modeling of Rock Fragmentation upon impact in Rock Fall Analysis. Rock Mechanics and Rock Engineering 44 (1), 23-35.

Fringes projection for 3D displacement analysis of experimental dry granular avalanches

Carlos Mares[1], Bernardino Barrientos-García[1], Mariano Cerca[2], Damiano Sarocchi[3], Luis Angel Rodriguez Sedano[4]

[1] *Centro de Investigaciones en Optica*
[2] *Centro de Geociencias, UNAM*
[3] *Instituto de Geología, UASLP*
[4] *Posgrado en Ciencias de la Tierra, UNAM*
e-mail: *mcerca@geociencias.unam.mx*
session: *Methods and Materials*

Introduction

Granular avalanches are common phenomena in nature, and when they occur on a large scale, represent major geological hazards (Dikau et al., 1996; Jakob and Hungr, 2005). Examples of granular avalanches are pyroclastic flows or debris flows (Sulpizio et al., 2010; Sarocchi et al., 2011). Experimental knowledge of the detailed kinematics of these phenomena is of great importance, because it allows developing more detailed rheological models, as well as more efficient simulation algorithms. Indirectly, the observations made in experiments can also contribute to an efficient hazard manage for civil protection.

The method proposed here allows a study over time, at high-speed, of the three-dimensional evolution of a dry- experimental avalanche body. Such study provides more detailed information on grain size segregation and velocity changes inside the avalanche during its development. We present a variation of the optical method based on fringes projection that allows obtaining full field 3D displacements for a model surface by analyzing color images (Barrientos et al., 2008; Mares 2011). The three deformation components are obtained by decomposing the spatial information in the three color channels (RGB). The advantages of this technical variation include that the finite deformation components on- and out-of-the plane are obtained simultaneously (in only one image), and thus it can be applied to fast laboratory processes (fractions of second).

Experimental setup and methods

The experimental granular materials simulating avalanches were made of natural mixtures of volcanic materials with monodispersal and polidispersal grain sizes, and the physical experiments were performed in two different flumes of 1 and 5.5 m long.

The small flume consist of a plexiglass ramp with inclination of 42° and with lateral confining walls. A mixture of low density granular material (pumice) of 1.5 kg was thrown in the upper part of the ramp and monitored by the fringe projection technique. The mean velocity on the ramp plane was of ca. 2.2 m/s.

For the analysis of the granular flow in the small flume a colored (green) fringe pattern with a 6.45 mm period was projected on the ramp, using a high definition Panasonic PT-AE2000 projector and digital images were recorded using a Photron MiniUX100 camera at a frame rate of 1000 images per second. The optical setup for resolving the relief of the flow is presented in figure 1.

Both the camera and the projector were placed

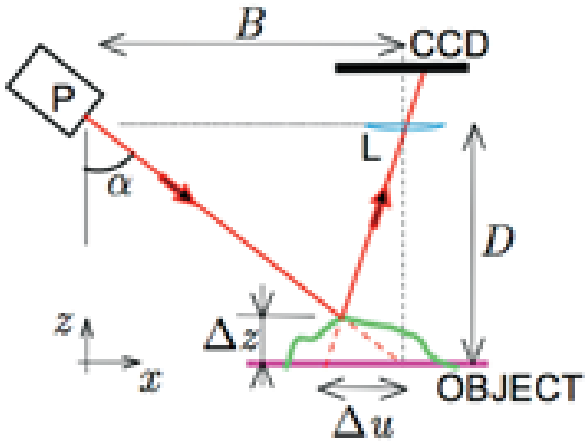

Fig. 1.: Optical set up.

at the same distance from the ramp (1050 cm) and the angle among the camera and the projector was 14.7°. The camera was placed perpendicular to the ramp plane and the total area of analysis was of 710×105 mm2. The images recorded were decomposed in channels R, G, and B. The G channel image contains the information needed to compute the fringe analysis and out-of-plane deformation whilst pairs of the R channel images were cross correlated to obtain the in-plane displacement.

The large flume is equipped with a series of sensors for kinematic, pressure, sound and high speed video analysis. The information from the analysis with the fringes method, supplemented with data provided by the large flume sensors, allow interesting insights about the processes governing granular avalanches.

Results

Results of the granular flow in the small flume are shown in figures 2, 3, and 4. The total experimental time was 1800 milliseconds. Figure 2 presents the out-of-the plane deformation using a red-blue color scale and taking the experimental ramp as the reference plane. Occasionally during the experiment two horizontal bands appear that artifacts of the Fourier method unrelated to flow. Height values (mm) are referred to the initial inclined plane.

Figure 3 is the difference of the out-of-plane deformation computed among two images separated by 2 milliseconds. These results allow to visualize small changes in height during flow and highlight the activity of the deformation front before 360 milliseconds.

Figure 4 is a summary of the kinematics of the experiment. In figure 4a, mz is the height of the flow and can be seen as a measure of the granular material volume in the flume, which is maximum at 380 milliseconds. The flume is filled with the material for about 30 milliseconds and posteriorly the volume decreases.

In sdz (Figure 4a) is shown the evolution of the standard deviation of the displacements. At the beginning of the flow the displacement of particles in the front is characterized by rolling and saltation and their chaotic behavior induce a high variability in the measurements. The maximum variability is observed to end at 400 milliseconds when the flow front reaches the right end of the inspected area. The width of the front increases through its displacement from left to right implying a greater area with unstable particles and a higher standard deviation of the measurement. From 400 to 800 milliseconds the flume is full of material and the flow reaches a laminar and partially steady state. Between 800 and 1400 milliseconds there is an unstable discharge tail of the flow that causes again an increment of the standard deviation of the measurements. The length of the tail increases gradually and the unstable displacement reaches a maximum at 1400 milliseconds. Later, the standard deviation decreases with the flow waning.

MAX (figure 4a) is the maximum deformation and was computed by the average of the 5000 pixels with the largest values of deformation at a given time. The maximum deformation was obtained at 180 milliseconds and then the flow stabilizes. Decreasing of the maximum deformation might be associated to granular segregation of the front. A slight increase is observed again at 1000 milliseconds associated probably to flow tail.

Figure 4b, mdz in the average of the deform-

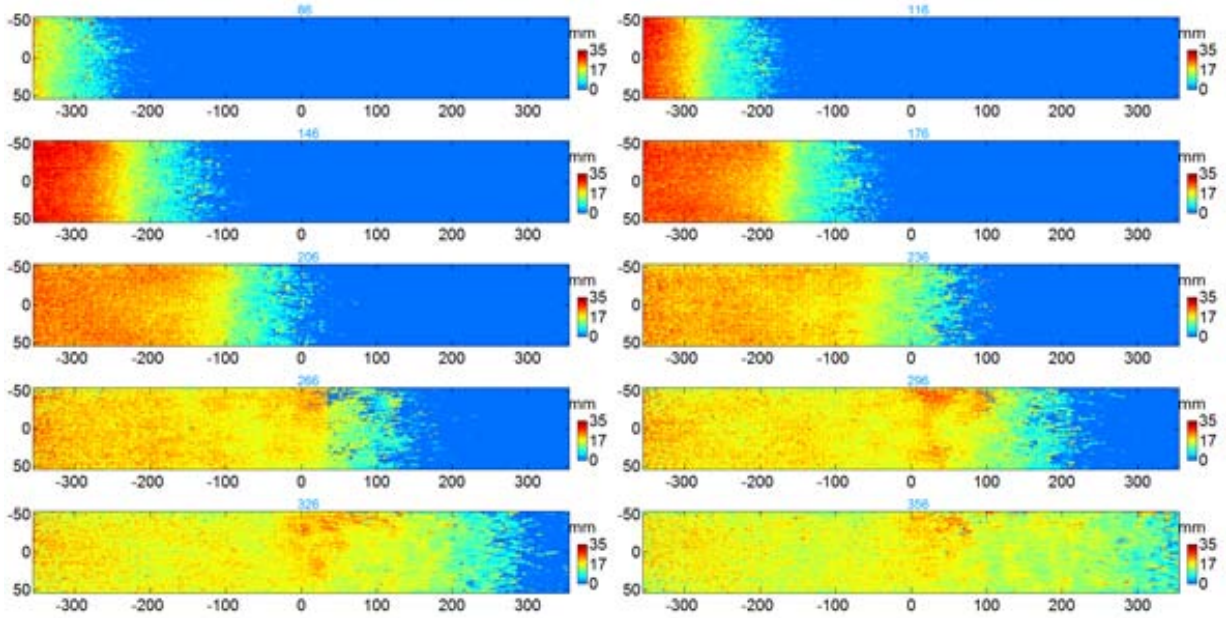

Fig. 2.: Position (mm) vs height (mm) in color of the experimental avalanche. The label in blue indicates the time of the image (in milliseconds).

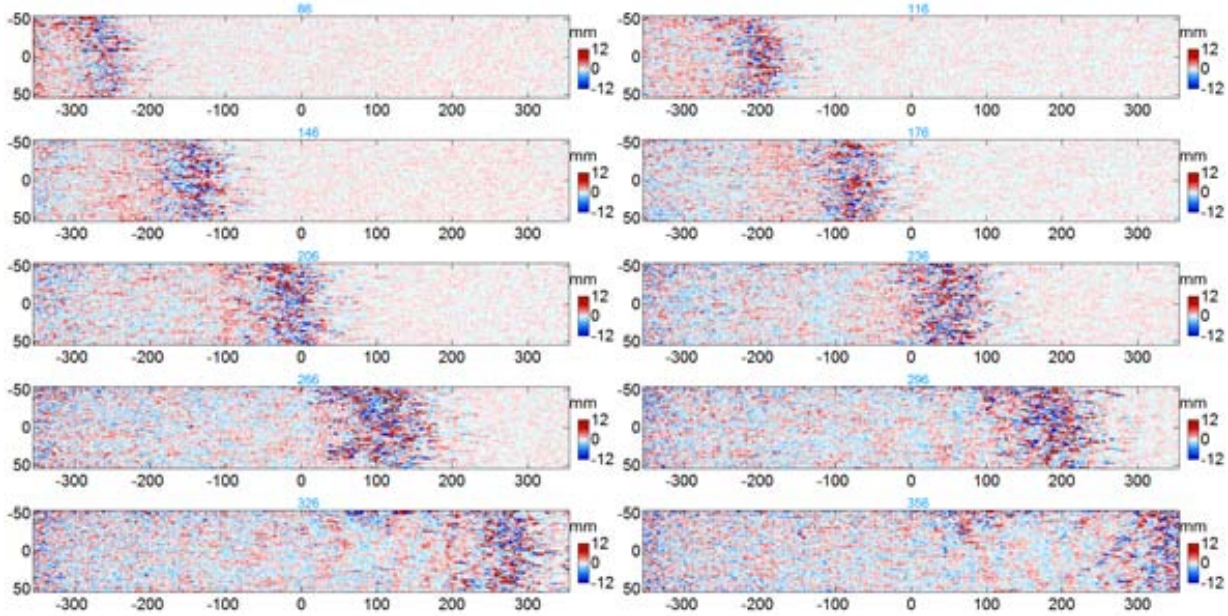

Fig. 3.: Difference of the out-of-plane deformation, obtained by comparison among two images separated by 2 milliseconds.

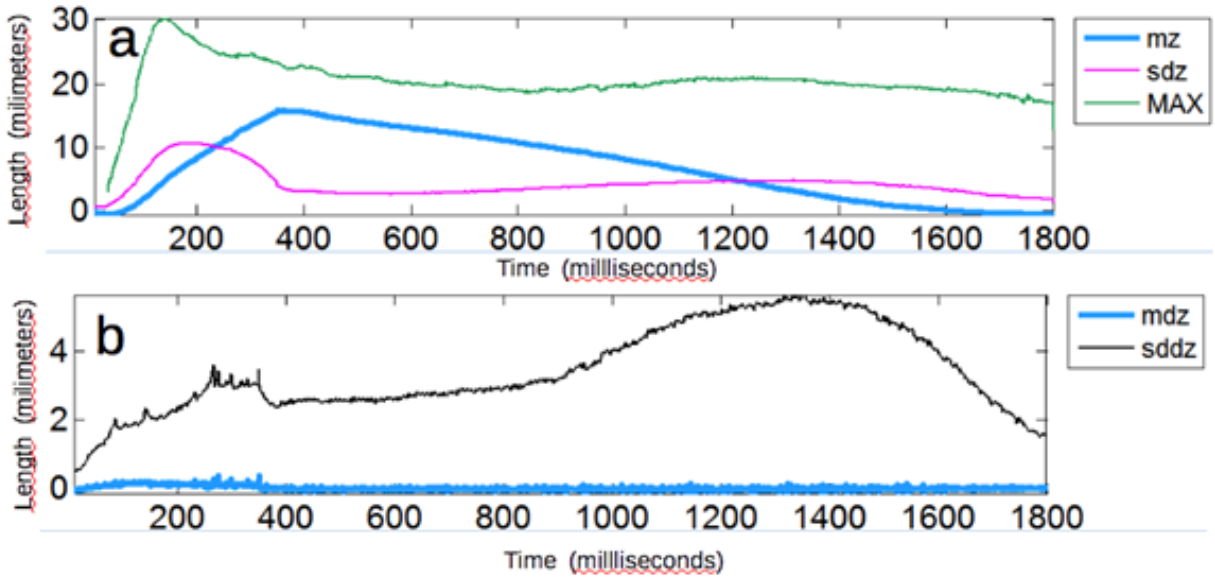

Fig. 4.: (a) mz, height of the flow in mm; sdz, standard deviation of the displacements (mm); MAX maximum deformation (mm). (b) mdz, average of the deformation differences; sdz, standard deviation of the deformation differences.

ation differences that increases gradually up to 400 milliseconds. As in the case of the maximum deformation is associated to the unstable (rolling and salting) particles of the front and tail of the flow. A better image of the unsteady flow particles is shown by the sdz, which is the standard deviation of the deformation differences. The largest values are conspicuously associated to the front and tail of the flow that are the states of greatest instability.

Figure 5 shows a summary of the PIV computed for the first 360 milliseconds of the experiment. The higher velocity is related to the front of the flow. Note that the difference in maximum and minimum velocity increases as the flow evolves.

Finally, we conclude that the optical method based on fringes projection and cross correlation of images is a suitable method allowing to obtain the full field 3D displacements of a granular avalanche. This study provides detailed information on grain size segregation and velocity changes inside the avalanche during its development.

References

Barrientos, B., Cerca, M., García-Márquez, J., and Hernández-Bernal, C. 2008. Three-dimensional displacement fields measured in a deforming granular-media surface by combined fringe projection and speckle photography. Journal of Optics A: Pure and Applied Optics 10 (10), 104027

Dikau, R., Brunsden, D., Schrott, L., Ibsen, M.L. 1996. Landslides recognition. Ed. John Wiley & Sons. 251 p.

Jakob and Hungr. 2005. Debris-flow Hazards and Related Phenomena. Ed. Springer, 738 p.

Mares, C., Barrientos, B., & Blanco, A. 2011. Measurement of transient deformation by color encoding. Optics express, 19(25), 25712-25722.

Sarocchi, D., Sulpizio, R., Macías, J.L., Saucedo, R. 2011. The 17 July 1999 block-and-ash flow at Colima volcano: new insights on volcanic granular flows from textural analysis. (ISSN: 0377-0273). Journal of Volcanology and Geothermal Research. 204: 40-56. http://dx.doi.org/10.1016/j.jvolgeores.2011.04.013

R. Sulpizio, L. Capra, D. Sarocchi, R. Saucedo, J.C. Gavilanes, N. Varley. 2010. Predicting the block and ash flow inundation areas at Fuego de Colima volcano (Colima, Mexico) based on the present day status. Journal of Volcanology and Geothermal Research. 193: 49-66.

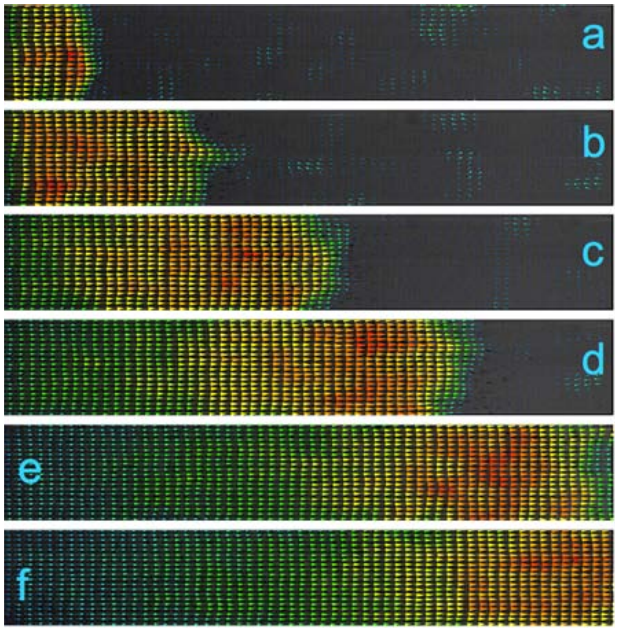

Fig. 5.: Description of the instantaneous velocimetry of the flow from the displacements obtained by the cross-correlation of pair of images separated by 2 millisecond: (a) 65 ms, max velocity 2.2 m/s (red colors), min velocity 0.9 m/s (green colors), (b) 130 ms, max 2.5 m/s, min 0.92 m/s, (c) 195 ms, max 2.7 m/s, min 0.8 m/s, (d) 260 ms, max 2.7 m/s, min 0.92 m/s, (e) 325 ms, max 2.93 m/s, min 0.4 m/s, (f) 350 ms, max 3 m/s, min 0.55 m/s.

A 3-D Lagrangian finite element algorithm with contour-based re-meshing for simulating large-strain hydrodynamic instabilities in visco-elastic fluids

Marina von Tscharner[1], Stefan Schmalholz [1]

[1] *Université de Lausanne, Institut des sciences de la Terre, Quartier UNIL-Mouline, Bâtiment Géopolis, CH-1015 Lausanne*
e-mail: *marina.vontscharner@unil.ch*
session: *Methods and Materials*

Many three-dimensional (3-D) structures in rock, which formed during the deformation of the Earth's crust and lithosphere, are controlled by a difference in mechanical strength between rock units and are often the result of a geometrical instability. Such structures are, for example, folds, pinch-and-swell structures (due to necking) or cuspate-lobate structures (mullions). These structures occur from the centimeter to the kilometer scale and the related deformation processes control the formation of, for example, fold-and-thrust belts and extensional sedimentary basins or the deformation of the basement-cover interface. The 2-D deformation processes causing these structures are relatively well studied. However, several processes during large-strain 3-D deformation are still incompletely understood. One of these 3-D processes is the lateral propagation of these structures, such as cusp propagation in a direction orthogonal to the shortening direction or neck propagation in direction orthogonal to the extension direction. We study the 3-D evolution of geometrical instabilities with numerical simulations based on the finite element method (FEM). Simulating geometrical instabilities caused by sharp variations of mechanical strength between rock units requires a numerical algorithm that can accurately resolve material interfaces for large differences in material properties (e.g. between limestone and shale) and for large deformations. Therefore, our FEM code combines a numerical contour-line technique and a deformable Lagrangian mesh with re-meshing. With this combined method it is possible to accurately follow the initial material contours with the FEM mesh and to accurately resolve the geometrical instabilities. The algorithm can simulate 3-D deformation for a visco-elasto-plastic rheology. Stresses are limited by a yield stress using a visco-plastic formulation and the viscous rheology is described by a power-law flow law. The 3-D FEM code is applied to model 3-D power-law folding and power-law Rayleigh-Taylor instabilities (diapirs) with different re-meshing scenarios. The results are tested with the analytical solution for small amplitudes and with 2-D numerical results for large amplitudes. Thereby, the small initial geometrical perturbations for folding and necking are exactly followed by the FEM mesh. In order to test and measure the numerical properties for an Eulerian mesh we use the analytical solution for a two-dimensional viscous inclusion in pure shear (Fig. 1). We present high resolution 2-D (i.e. cylindrical 3-D with only one element in the third direction) and moderate resolution 3-D results that are applied to the formation of fold nappes (Fig. 2) and to necking during slab detachment (Fig. 3).

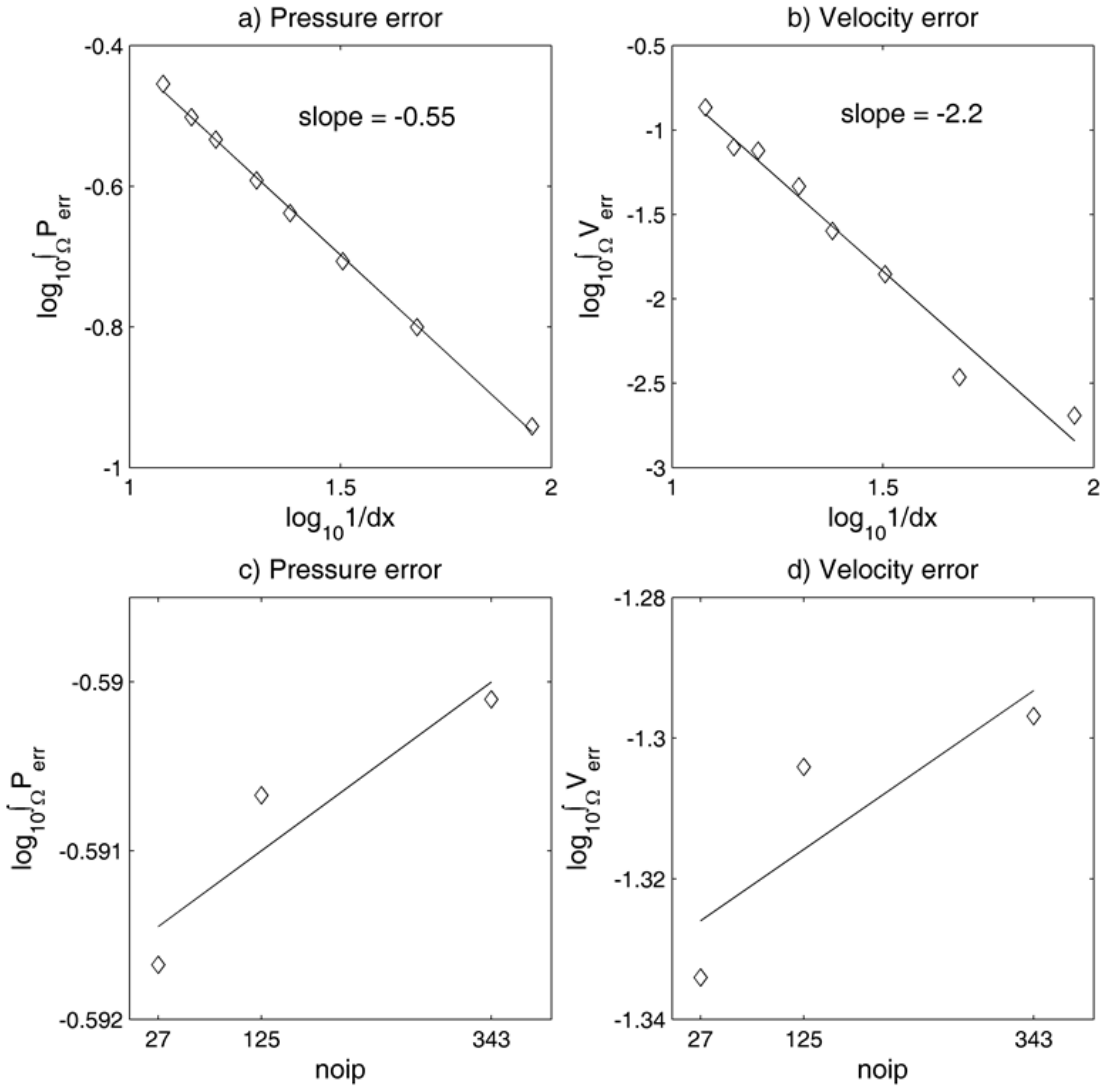

Fig. 1.: Convergence test for a rigid viscous inclusion in a weak matrix under pure shear. Integrated error in pressure and velocity over the model domain versus the nodal FEM resolution (a and b) and versus the number of integration points per element (c and d). We us either $27 = 3^3$,$125 = 5^3$ or $343 = 7^3$ integration points.

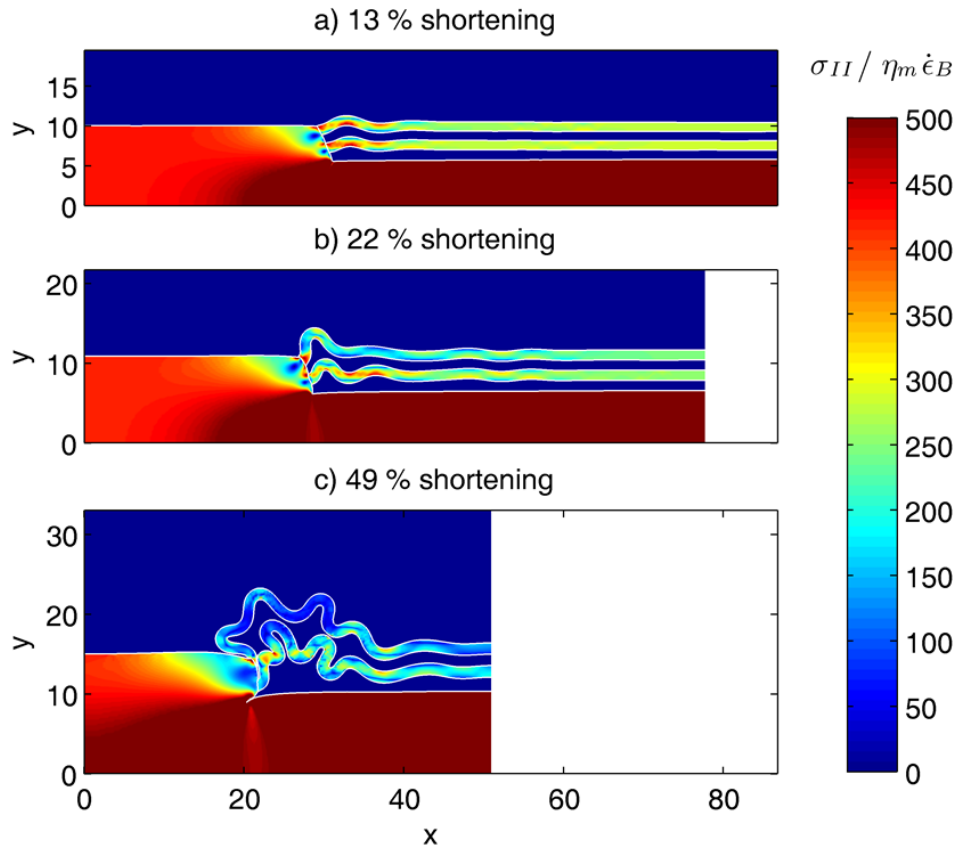

Fig. 2.: Geometrical evolution for fold nappe formation for 13, 22 and 49% shortening. The colors indicate the distribution of dimensionless second invariant of stress tensor. The competent sedimentary layers are first buckeled and then sheared over the basement to form a recumbent fold nappe.

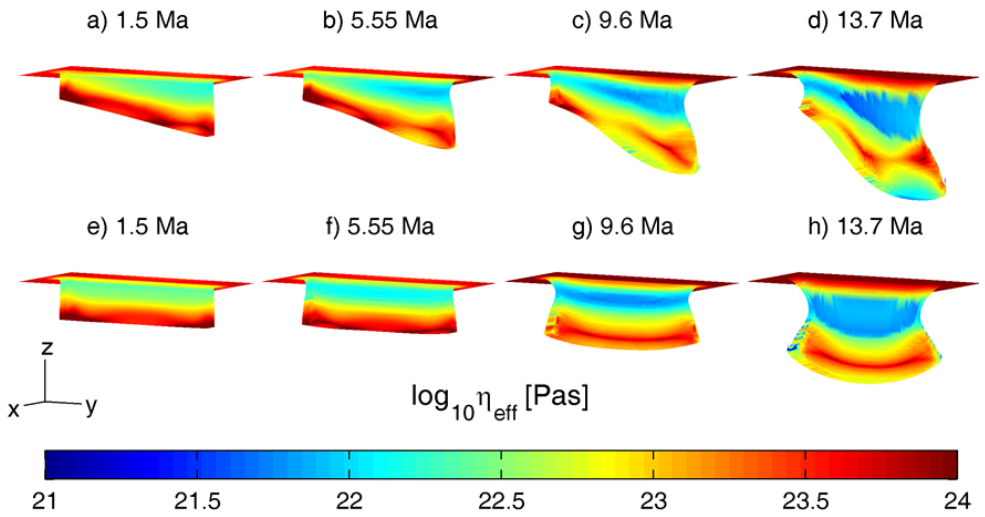

Fig. 3.: The 3-D geometric evolution of an initially symmetric (a-c) and asymmetric (d-f) slab of 800 km width for different times. The colors on the slab surface indicate the effective viscosity in Pa.s.

Some Remarks on wet gypsum as a viscous material for physical modeling

Ali Yassaghi[1]

[1] *Department of Geology, Tarbiat Modares University, P.O. Box 14115-175, Tehran, Iran*
e-mail: *yassaghi@modares.ac.ir*
session: *Methods and Materials*

Dry sand, wet clay and silicone polymers are most common modeling materials in physical modeling (Eisenstadt et al., 1995). Typically, the sand and clay represent competent (brittle rocks), whereas the silicone polymers simulate incompetent (ductile rocks). In this paper we present remarks on application of wet gypsum to simulate mechanical behavior of ductile rocks in modeling deformed structures. For this, physical modeling in which wet gypsum and wet clay are used as modeling material are presented to model folding and fracturing. This study is not intended to represent development of any particular natural geological structures, but to recommend wet gypsum as a ductile analogue material.

Dry gypsum powder (plaster of Paris) has been used to simulate tensile fractures and faults (e.g., Gabrielsen and Clausen, 2001). The viscosity of wet gypsum, however, is less than normal gypsum plaster. This is because, it prepares by simultaneously adding water and shaking that cause to slow down drying time from few minutes to more than a day. Thus, it can be used as ductile material for physical modeling (Fig. 1). In our physical modeling, wet clay considered as competent material and wet gypsum as incompetent material. This is because they both have the advantage to sustain open fractures, and when the water contents can be carefully controlled, the material properties can be controlled to some extent. The chief technical limitations of applying wet gypsum are the influence of the modeling sidewalls and the difficulties that arise by filling the box. Increasing the size of the model set-up will reduce the effects of the sidewalls.

Fig. 1.: Wet gypsum as ductile material in physical modeling.

For analogue modeling of folds, wet gypsum plaster is used with wet clay in order to accommodate competence contrast necessary for development of folds. Variation of the wet gypsum thickness, as ductile material, controls the style of folding from surface to depth (Fig. 2), as well as its behavior to act as detachment horizon during folding (Fig. 3). The resultant structures similar to various detachment folds develop in fold-thrust belts. In addition, applying various thickness of wet clay while keeping the thickness of wet gypsum, results in change on fold geometry from harmonic for the case of constant clay thickness (Fig. 4a) to polyharmonic for the case of various clay thickness (Fig. 4b). This shows that the wet clay can act as competent material during the folding.

For study of fractures wet gypsum allows to understanding fault growth processes and to detect areas of high small-scale strain such as fault

Fig. 2.: Variation of wet gypsum as viscous material on fold style from surface to depth.

Fig. 3.: The effect of wet gypsum to act as detachment horizon during folding.

Fig. 4.: Harmonic(a) and polyharmonic folding (b).

linkage zones. Various tensile and shear fractures is develop on the wet gypsum during shortening. Pull apart and push up are common structures develop along the shear fractures that are comparable with the natural examples. However, fractures are less developed in wet gypsum than wet clay reflecting the marked difference in viscosity of wet gypsum with respect to wet clay (Fig. 6).

References

Gabrielsen, R.H., and Clausen, J.A., 2001, horses and duplexes in extentional regimes: A scaled-modeling contribution, in Koyi, H.A., and Mancktelow, N>S., eds,Tectonic Modeling : a volume in in Honor of Hans Ramberg. Geological Society of America, Memoir, vol. 193, pp. 207-220.

Eisenstadt, G., Vendeville, B.C., Withjack, M.O., 1995. Introduction to Experimental Modeling of Tectonic Processes. Continuing Education Course Notes. Geological Society of America, unpaginated.

Fig. 5.: development of tensile and shear fractures in wet gypsum.

Fig. 6.: Showing the greater development of fractures in wet clay than wet gypsum.

Scientific Programme

GeoMod2014 - Conference Outline

Time	31. August	1. September	2. September	3. September
08:45 - 09:00	-	Welcome	-	-
09:00 - 11:00	-	(Seismo-)tectonics (orals)	Volcanism and Volcanotectonics (orals)	Rheology (orals)
11:00 - 13:00	-	(Seismo-)tectonics (posters)	Volcanism and Volcanotectonics (poster)	Rheology (poster)
13:00 - 14:00	-	Lunch break	Lunch break	Lunch break
14:00 - 16:00	-	Tectonics and Surface processes (orals)	Geodynamics (orals)	Fluids and Deformations (orals)
16:00 - 18:00	-	Tectonics and Surface processes (poster)	Geodynamics (posters)	Fluids and Deformations (poster)
18:00 - 21:00	Ice Breaker Party	-	-	-
19:00 - 22:00	-		Joint Conference Dinner	-

GeoMod2014 - Short course on "Constitutive Laws: from Observation to Implementation in Models" by Onno Oncken, Mathias Rosenau, Fabio Corbi, Georg Dresen Erik Rybacki, Stephan Sobolev, and Sascha Brune
Thursday 4 September: 09:00 - 18:00
Friday 5 September: 09:00 - 14:00

GeoMod2014 - Hands-on tutorial on "ASPECT: a next-generation geodynamic modelling software" by Anne Glerum and Juliane Dannberg
Thursday 4 September: 09:00 - 18:00: Tutorial
Friday 5 September: 09:00 - 18:00: ASPECT Strategy Workshop (for Advanced Users) - voluntary

GeoMod2014 Conference Programme (31 August - 3 September)

Sunday 31 August 2014

18:00 - 21:00: Ice Breaker Party at the 'Theaterschiff Potsdam' (Schiffbauergasse 9b, 14467 Potsdam)

Monday 1 September 2014

08:45 - 09:00: Welcome by Prof. Dr. Dr. h.c. Reinhard Hüttl and Prof. Dr. Onno Oncken

09:00 - 11:00: (Seismo-)tectonics Orals (chairs: B. Kaus, O. Oncken)

- 09:00 - 09:30: **Kelin Wang:** *Thermal Expressions of Stick-slip and Creeping Subduction Megathrusts* (keynote)
- 09:30 - 10:00: **Bertrand Maillot:** *The long-term Evolution of Fold-and-Thrust Belts: Consistency of Numerical Approaches and Physical Experiments* (keynote)
- 10:00 - 10:20: **Tasca Santimano** et al.: *Smart or Beautiful? Accretionary wedge evolution seen as a competition between minimum work and critical taper*
- 10:20 - 10:40: **Lorenzo Bonini** et al.: *The role of pre-existing frictional weaknesses on the propagation of extensional faults*
- 10:40 - 11:00: **Ylona van Dinther** et al.: *Seismo-thermo-mechanical modeling of subduction zone seismicity*

11:00 - 13:00: (Seismo-)tectonics Posters (chairs: B. Kaus, O. Oncken)

13:00 - 14:00: Lunch break

14:00 - 16:00: Tectonics and Surface processes Orals (chairs: F. Graveleau, N. Hovius)

- 14:00 - 14:30: **Ritske Huismans:** *Interaction and feedback between surface processes and mountain building* (keynote)
- 14:30 - 15:00: **Stéphane Dominguez:** *Joint analogue modelling of marine and terrestrial geological processes: state of the art and new developments* (keynote)
- 15:00 - 15:15: **Utsav Mannu** et al.: *Dynamic Modelling of Accretionary Prisms and Stratigraphy of Forearc basins*
- 15:15 - 15:30: **Karen Leever:** *3D Analogue Modelling of the Effect of Fan Sedimentation on Accretionary Wedge Dynamics – the Magdalena Fan case, South Caribbean Margin, Colombia*
- 15:30 - 15:45: **Frank Zwaan**, Guido Schreurs: *4D Transfer Zone Modeling in Continental Rift Systems*
- 15:45 - 16:00: **Sergei Medvedev**, Ebbe H. Hartz: *Evolution of topography of post-Devonian Scandinavia: Effects and rates of erosion*

16:00 - 18:00: Tectonics and Surface processes Posters (chairs: F. Graveleau, N. Hovius)

Tuesday 2 September 2014

09:00 - 11:00: Volcanism and Volcanotectonics Orals (chairs: O. Galland, E. Holohan)

- 09:00 - 09:30: **Rikke Pedersen:** *Surface deformation simulations of volcanic and tectonic processes in Iceland* (keynote)
- 09:30 - 10:00: **Olivier Roche**, Yarko Niño: *Mechanisms of entrainment of a granular substrate by pyroclastic density currents: insights from laboratory experiments and models, and implications for flow dynamics* (keynote)
- 10:00 - 10:15: **Rosanne Heistek** et al.: *Temporal changes in mantle wedge geometry and magma generation processes in the Central Andes: towards linking petrological data to thermomechanical models*
- 10:15 - 10:30: **Francesco Maccaferri** et al.: *The gravitational unloading due to rift depression: A mechanism for the formation of off-rift volcanoes in (continental) rift zones*
- 10:30 - 10:45: **Lola Chanceaux**, Thierry Menand: *Solidification effects on sill formation: an experimental approach*
- 10:45 - 11:00: Max Gallagher, **Ben Kennedy** et al.: *Megatsunami generation from caldera subsidence*

11:00 - 13:00: Volcanism and Volcanotectonics Posters (chairs: O. Galland, E. Holohan)

13:00 - 14:00: Lunch break

14:00 - 16:00: Geodynamics Orals (chairs: F. Funiciello, S. Sobolev)

- 14:00 - 14:30: **Anne Davaille:** *Plumes to Plate Tectonics: Insights from Laboratory Experiments* (keynote)
- 14:30 - 15:00: **Bernhard Steinberger** et al.: *On the relation between plate tectonics, large-scale mantle flow and mantle plumes: Some recent results and many open questions* (keynote)
- 15:00 - 15:15: **Paul J. Tackley** et al.: *Influence of Melting on the Long-Term Thermo-Chemical Evolution of Earth's Deep Mantle*
- 15:15 - 15:30: **Maria V. Chertova** et al.: *3-D numerical modeling of subduction evolution of the western Mediterranean region*
- 15:30 - 15:45: Tobias Baumann, **Boris Kaus**, A. Popov: *Constraining the rheology of the lithosphere through geodynamic inverse modelling*
- 15:45 - 16:00: **Elisa Calignano** et al.: *Strain localization during compression of a laterally heterogeneous lithosphere*

16:00 - 18:00: Geodynamics Posters (chairs: F. Funiciello, S. Sobolev), Methods and Materials Posters (chairs: M. Frehner, M. Rosenau)

19:00 - 22:00 Joint conference dinner in Potsdam on the ship 'Belvedere' (Lange Brücke 6, 14467 Potsdam)

Wednesday 3 September 2014

09:00 - 11:00: Rheology Orals (chairs: G. Dresen, H. Sone)

- 09:00 - 09:30: **Yuri Fialko:** *Numerical models of ductile roots of mature strike-slip faults* (keynote)
- 09:30 - 10:00: **Laurent Montési:** *Localization processes on Earth, Mars, and Venus* (keynote)
- 10:00 - 10:20: **Suzon Jammes** et al.: *Localization of deformation in a polymineralic material*
- 10:20 - 10:40: **Sebastian P. Müller** et al.: *Rheology of bubble- and crystal-bearing magma: new analogue experimental data and an effective-medium model*
- 10:40 - 11:00: **Maria A. Nikolinakou** et al.: *Modeling stress evolution around a rising salt diapir*

11:00 - 13:00: Rheology Posters (chairs: G. Dresen, H. Sone)

13:00 - 14:00: Lunch break

14:00 - 16:00: Fluids and Deformations Orals (chairs: S. Miller, M. Moreno)

- 14:00 - 14:30: **Boris Galvan** et al.: *Towards a general simulation tool for complex fluid-rock lithospheric processes: merging pre-processing, processing and post-processing in state-of-the-art computational devices* (keynote)
- 14:30 - 15:00: **Takeshi Tsuji:** *Digital rock physics: Insight into fluid flow and elastic deformation of porous media* (keynote)
- 15:00 - 15:15: **Thomas Heinze** et al.: *Numerical Modelling of earthquake swarms in the Vogtland / West- Bohemia*
- 15:15 - 15:30: **Samuel Angiboust** et al.: *Effect of Fluid Circulation on Intermediate-Depths Subduction Dynamics: From Field Observations to Numerical Modelling*
- 15:30 - 15:45: Magdalena Scheck-Wenderoth, **Judith Sippel** et al.: *Heat transport mechanisms at different scales – a 3D modelling workflow*
- 15:45 - 16:00: **Antoine Jacquey** et al.: *Modelling of fractured reservoirs: Fluid-rock interactions within fault domains*

16:00 - 18:00: Fluids and deformations Posters (chairs: S. Miller, M. Moreno)

The posters will be presented during the entire conference. Each poster session starts with a 1-2 min. short presentation of all participating posters.

GeoMod2014 - Short course on "Constitutive Laws: from Observation to Implementation in Models"

Thursday 4 September 2014

Morning Session: Onno Oncken, Mathias Rosenau, and Fabio Corbi

- 09:00 - 10:00: **Onno Oncken:** Observing deformation kinematics and localization: Observations from the field, geophysical imaging, and geodetic monitoring
- 10:00 - 10:15: Coffee Break
- 10:15 - 11:00: **Mathias Rosenau:** Rheology of rock analogues 1: Elastoplasticity and its application in seismotectonic simulation
- 11:00 - 11:15: Coffee Break
- 11:15 - 12:00: **Fabio Corbi:** Rheology of rock analogues 2: Viscoelasticity and its application in seismotectonic simulation
- 12:00 - 13:00: **Visit to the GFZ Analogue Lab**

13:00 - 14:00: Lunch break

Afternoon Session: Georg Dresen and Erik Rybackii

- 14:00 - 15:15: Rheology of the lower crust : Reconciling laboratory data and field observations
- 15:15 - 15:30: Coffee Break
- 15:30 - 16:45: **Visit to the GFZ rock mechanics lab**
- 16:45 - 17:00: Coffee Break
- 17:00 - 18:00: Rock fracture processes and stick slip sliding –What do we learn from analyzing nanofemto seismicity?

Friday 5 September 2014

Morning Session: Stephan Sobolev and Sascha Brune

- 09:00 - 10:00: **Stephan Sobolev:** Rheology and geodynamic modeling: key controls in plate tectonics and beyond
- 10:00 - 10:15: Coffee Break
- 10:15 - 11:30: **Sascha Brune:** Rock rheology in numerical models: PC exercises and application to rift dynamics
- 11:30 - 11:45 Coffee Break
- 11:45 - 12:30: **Stephan Sobolev:** Rheology and cross-scale modeling: towards understanding of great earthquakes
- 12:30 - 13:00: Discussion

13:00 - 14:00: Lunch and end of the short course

GeoMod2014 – Hands-on tutorial on"ASPECT: a next-generation geodynamic modelling software" by Anne Glerum and Juliane Dannberg

Thursday 4 September 2014

08:30 - 9:00: Registration

- 09:00 - 10:00: **Tutorial 1:** First Steps – Compiling and Running ASPECT, **Lecture:** How to run and visualize simple models
- 10:00 - 11:15: **Lecture** ASPECT – A next-generation geodynamic modelling software, **Tutorial 2:** Convection in a 2D box
- 11:15 - 11:30: Coffee Break
- 11:30 - 13:00: **Tutorial 3:** Using the adaptive mesh refinement and spherical shell geometry **Lecture:** How to run and visualize simple models

13:00 - 14:00: Lunch break

- 14:00 - 15:15: **Tutorial 4:** Using the adaptive mesh refinement and spherical shell geometry and using the function parser
- 15:15 - 15:30: Coffee Break
- 15:30 - 17:00: **Tutorial 5:** Averaging at the example of subduction and using a “sticky air” layer
- 17:00 - 18:00: **Voluntary:** Installing ASPECT on personal computers

18:30: Joint Dinner (to be payed by the participants)

Friday 5 September 2014

09:00 - 18:00: ASPECT Strategy Workshop for Advanced Users: Perspectives for Modelling with ASPECT

Index